Politecnico di Torino
Dottorato di Ricerca in Fluidodinamica
XIII Ciclo

Tesi di Dottorato

Angular momentum applications in fluid mechanics

Michele Iovieno

Marzo 2001

Index

Introduction

We consider in this thesis the applications of the angular momentum budget in fluid dynamics problems. The two main situations in which a balance of angular momentum is worthwhile to be considered, that is structured flows and a homogeneous fluid when balances on finite volumes are introduced, are discussed in chapter 1.

The first situation arises when one deals with a non homogeneous fluid with internal structures on which external forces and couples may act, as liquid crystals, blood flow or dusty plasmas (Batchelor, 1970) or granular media (Cercignani & Lampis (1988), Goldshtein & Shapiro (1995)). In these cases the angular momentum budget is no more equivalent to the momentum budget and a new variable, the intrinsic angular momentum per unit volume, must be brought in.

In the latter case, the equation for the intrinsic moment of momentum averaged over finite fluid volumes is considered. A new representation of it in terms of an infinite sequence of independent equations by means of a series expansion in terms of the linear dimension of the volumes is introduced, extending earlier deductions by Nigmatulin & Nikolaevsky (1970) and Chatwin (1973). The first order term is just the Helmholtz equation while the remaining terms can be viewed as balances for a kind of higher order vorticities.

Applications to turbulence of angular momentum balance are then considered (Mattioli (1933), Nikolaevsky (1970), Nikolaevsky (1973), Eringen (1972)). Since Mattioli's earliest application in 1933, the equations of motion were often integrated over finite volumes to evidence the evolution of the large scales of turbulence. Even with fluids deprived of internal structures, asymmetry was associated to the turbulent stress in Mattioli (1933, 1937) and in Nicolaevsky (1970, 1973). In Eringen (1972) the micromorphic theory of structured media was applied to turbulence. In all these approaches, the balance equations for momentum and angular momentum are coupled.

It will be shown that this coupling, based on a supposed antisymmetric part of the stress tensor, is devoid of physical rationale. However, starting from the analysis of the structure of the angular momentum budget over finite volumes, and from the scaling law of turbulent diffusion, a new large eddy model, based on the use of angular momentum to represent turbulent transport, is proposed in chapter 2. In this model the coupling is given by a functional dependence of the turbulent eddy diffusivity over the angular momentum of a finite volume of fluid. Even if it is proposed and subsequently validated mostly in the framework of incompressible turbulence, it is thought also for possible applications to flows containing suspended particles with inertia and on which external couples may act, for which an intrinsic angular momentum equation must be always taken in account. Its validation comprehends standard tests, which include not only the *a priori* test (Clark et al. (1979)) and the simulation of homogeneous decaying turbulence, but also the analysis of a particular class of turbulent mixings, characterized by the absence of mean shear. In this special configuration the two turbulent flows that are going to mix differ in the turbulent kinetic energy.

Results present in literature about shearless mixings, either coming from grid turbulence experiments (Veeravalli & Warhaft (1989)) and from direct numerical simulation (Briggs et al. (1996)) are reproduced by means of this new angular momentum model. Moreover, new results are presented in chapter 3 for a wider range of cases, in which the two turbulence fields that are going to mix differ also in their spectral content. The fundamental role of the gradient of an integral scale gradient, adverse or concurrent to the gradient of kinetic energy, on the global characteristics of this class of mixings is shown. This latter investigation might be of interest in gaining new information and insight in the turbulent self-interaction processes.

Chapter 1

Angular momentum and symmetry

1. Introduction

In continuum mechanics the angular momentum balance is usually considered only in the discussion of the symmetry of the stress tensor. The angular momentum of a continuum mechanics material point is of course taken as $\mathbf{x} \wedge \rho\mathbf{u}$ because a point has no dimension. In this way it has only a transport term and no intrinsic angular momentum for the motion relative to its centre of mass. From this it follows that the angular momentum balance is the moment of the momentum balance plus the antisymmetric part of the stress tensor. In fact, see for example Gurtin (1981), the budget of angular momentum is

$$\frac{\mathrm{d}}{\mathrm{d}t}\int_{A(t)} \varepsilon_{ijk} x_j \rho u_k \mathrm{d}\mathbf{x} = \int_{\partial A(t)} \varepsilon_{ijk} x_j T_{km} n_m \mathrm{d}\sigma + \int_{A(t)} \varepsilon_{ijk} x_j \rho b_k \mathrm{d}\mathbf{x} \qquad (1.1)$$

where T_{ij} is the macroscopic stress tensor, b_i the density of external body forces and $\varepsilon_{i\ell k}$ Ricci's alternating tensor. From (1.1) it is obtained

$$\mathrm{D}_t(\varepsilon_{ijk} x_j \rho u_k) = \varepsilon_{ijk} T_{jk} + \varepsilon_{ijk} x_j \partial_m T_{km} + \varepsilon_{ijk} x_j \rho b_k$$

and, after the moment of the momentum balance equation is subtracted, this yields to

$$\varepsilon_{ijk} T_{jk} = 0 \qquad (1.2)$$

that is, the antisymmetric part of the stress tensor must vanish. This result has a counterpart in the kinetics theory by Boltzmann, where it is shown that the macroscopic stress tensor is obviously symmetric because the only

contribution is the inertial flow of momentum, that is $T_{ij} = \overline{u_i' u_j'}$, where u_i' is the velocity of molecular fluctuations respect to the mean motion.

However, there are some physical situations in which this representation of angular momentum is not satisfactory. To deal with a non-homogeneous fluid with internal structures on which external forces and couples act, it is necessary to introduce a different balance of angular momentum, in which the presence of an intrinsic angular momentum and of external couples affect the symmetry property of the stress tensor, see Batchelor (1970), Condiff & Dahler (1964), Dahler & Scriven (1963), Almog & Brenner (1999). In this case the moment of the momentum equation is no more equivalent to the angular momentum budget and a new variable, the intrinsic angular momentum per unit volume, must necessarily be brought in. This leads to a non trivial angular momentum balance equations, coupled with the momentum balance equation. The same appears dealing with granular flows, see Cercignani & Lampis (1988), Goldshtein & Shapiro (1995).

A continuum theory that attempts to account for these aspects is the micropolar theory (Eringen (1966), Eringen (1992), Łukaszewicz (1999)). This model views the medium as a collection of material systems, the micro-elements, owning momentum, intrinsic angular momentum and energy. The micro-elements may contain internal structures (like liquid crystals, blood cells,..), however the fluid is viewed as monophase. The motion of the microelement is fully described by the velocity of its centroid and by further continuous field functions which portray the internal motions of the element. In an incompressible flow Eringen's theory leads to a set of twelve differential equations, from which the intrinsic moment of momentum can be recovered by taking the antisymmetric part of the microgyration tensor. The equation of the intrinsic angular momentum appears to be coupled to the momentum equation expressed in terms of the centroid velocity in such a way as to establish a link between the intrinsic motion inside the microelements and the mean velocity field.

Moreover, during the last century the equation of angular momentum balance has been applied few times to discuss the behavior of turbulent flows. Since the earliest Mattioli's application in 1933, the equations of motion were often integrated over finite volumes to evidence the evolution of the large scales of the turbulence. Even with fluids deprived of internal structures, asymmetry was associated to the turbulent stress in Mattioli (1933, 1937) and in Nicolaevskii (1970, 1973). In Eringen (1972) the micromorphic theory was applied to turbulence.

An analysis about the structure of the angular momentum budget over finite volumes of linear dimension δ is carried out in §2 of this chapter. The

analysis is relevant to all situations where the fluid may be considered locally homogeneous. Through a power series development in the square of the linear dimension of average we show that the balance for the intrinsic momentum may be represented by an infinite succession of independent equations obtained applying linear antisymmetric operators to the momentum balance. The first order term of the sequence is the vorticity equation, as remarked also by Nigmatulin & Nikolaevsky (1970) and Chatwin (1973) while the higher order relations are not reducible to it and may be viewed as high order vorticity budgets.

In §3 the principal features of structured flows are discussed, with emphasis to the relevance of angular momentum balance.

Applications to turbulence of theories relevant to structured flows are discussed in §4 through the analysis of the symmetry property of the Navier-Stokes equations. The common aspects of these theories and their physical support are discussed. This discussion will be the basis for the argument of chapter 2, where, in the ambit of turbulence modeling, a different kind of coupling between the momentum and angular momentum turbulent equations, which does not rely on a supposed existence of the antisymmetric part of the stress tensor, is suggested. A large eddy scale model based on the proportionality of the turbulent diffusivity to the intrinsic moment of momentum will be proposed.

2. Angular momentum in space averaged flows

2. 1 Spatial averages

In the study of turbulence and of suspensions space averages are often introduced to eliminate the small scale turbulent fluctuations or the details of the motion around the suspended particles and anyway to isolate the features of the large scale behaviour. When applied to turbulent flows, this leads to the so called large eddy simulation. Even if it was first introduced in an atmospheric dynamics context by Smagorinsky (1963), and further developed and applied when the availability of computers made numerical computations feasible, it is not useless to remark that spatial averages applied to turbulence where first used by Reynolds in his works on pipe flows. Applications to turbulence are posted to the next sections. Here we shall briefly introduce the concept of spatial average and discuss its relation with angular momentum balance, together with some useful properties.

A simple spatial average may be defined in the following way: on a class

of sets defined by

$$\mathcal{I}_\delta = \{\boldsymbol{\eta} \in I\!R^3 : \| \boldsymbol{\eta} \| < \delta\}$$

we define an average operator $< \cdot >_\delta$ as

$$<f>_\delta (\mathbf{x}, t) = \frac{1}{V_\delta} \int_{\mathcal{I}_\delta} f(\mathbf{x} + \boldsymbol{\eta}, t) \mathrm{d}\boldsymbol{\eta} \tag{1.3}$$

where V_δ is the volume of $\mathcal{I}_\delta$ [1].

In large eddy simulation, spatial averages are normally defined as a convolution integral,

$$<f>_\delta = \int_{I\!R^3} f(\mathbf{y}) g(\mathbf{y} - \mathbf{x}; \delta) \mathrm{d}\,\mathbf{x}, \tag{1.4}$$

where function $g(\mathbf{x}; \delta)$ is a weight function, which implicitly defines the length scale δ of the average, even if a compact support is not required, and are often referred to as filtering (Germano (1992)). It is normally chosen with spherical symmetry, that is $g(\mathbf{x}) = \tilde{g}(\|\mathbf{x}\| \ \delta)$. This definition is the more general definition of a continuous space average operator. Let us consider any continuous linear operator $M : X_\Omega \to X_\Omega$, where Ω denotes here the flow domain and X_Ω is a dense subset of $L^2(\Omega)$, which associates to each function $f(\mathbf{x})$ its correspondent averaged function $(M[f])(\mathbf{x}) = <f> (\mathbf{x})$. We want to show that it may be written in the form (1.4). Let us fix $\mathbf{x}$ and consider the linear functional $\lambda_\mathbf{x} : X_\Omega \to I\!R$,

$$\lambda_\mathbf{x}[f] = (M[f])(\mathbf{x}) = <f> (\mathbf{x}),$$

that is, $\lambda_\mathbf{x}$ associates to each function f the value in $\mathbf{x}$ of the averaged function. Because of the linearity and continuity of $\lambda_\mathbf{x}$, there is an unique function ϕ such that

$$\lambda_\mathbf{x}[f] = (f | g_\mathbf{x})$$

that is

$$<f> (\mathbf{x}) = \int_\Omega f(\mathbf{y}) \phi(\mathbf{y}; \mathbf{x}) \mathrm{d}\mathbf{y}$$

where we have evidentiate the $\mathbf{x}$-dependence of function g. If M is a smoothing operator, we require that it preserves constant functions and that it is invariant to space translations, that is, $h(\mathbf{x}) = f(\mathbf{x} + \boldsymbol{\sigma})$ implies $<h> (\mathbf{x}) = <f> (\mathbf{x} + \boldsymbol{\sigma})$ for all vectors $\boldsymbol{\sigma}$. The latter condition leads to

$$\phi(\mathbf{y} - \boldsymbol{\sigma}; \mathbf{x}) = \phi(\mathbf{y}; \mathbf{x} + \boldsymbol{\sigma}) \quad \forall \mathbf{x}, \mathbf{y}, \boldsymbol{\sigma} \tag{1.5}$$

[1] When it does not create any trouble, index δ will be often omitted in averaged variables like $<f>_\delta$

that is obviously satisfied by $\phi(\mathbf{y};\mathbf{x}) = g(\mathbf{x}-\mathbf{y})$. It may be deduced with some further hyphotesis of regularity for ϕ: deriving with respect to σ_j and then putting $\boldsymbol{\sigma} = 0$, we have the wave equations

$$\frac{\partial}{\partial x_j}\phi(\mathbf{y},\mathbf{x}) + \frac{\partial}{\partial y_j}\phi(\mathbf{y},\mathbf{x}) = 0 \quad \forall j = 1,2,3$$

whose general solution is $\phi(\mathbf{y},\mathbf{x}) = g(\mathbf{x}-\mathbf{y})$. Moreover constant function invariance leads to the normalization condition

$$\int_\Omega g(\mathbf{y})\mathrm{d}\mathbf{y} = 1$$

Such spatial averages satisfy most of the properties that are required to an average operator in order to be a feasible instrument (Germano (1992)): it is linear and commutes with all partial derivatives. This last property may be easily verified by direct substitution in (1.4) if f and g are at least piecewise C^1 functions. It remains true also under weaker hypothesis, as it may be seen exploiting the continuity of the average operator or using, for example, the Fourier transform properties. It is well known (Rudin (1974)) that if $ik_j\hat{f}$ and $ik_j\hat{g}$ belong to L^1, then f and g are derivable and $\widehat{\partial_j f} = ik_j\hat{f}$, $\widehat{\partial_j g} = ik_j\hat{g}$. So, using also that $\widehat{f*g} = \hat{f}\hat{g}$, we have

$$(\widehat{\partial_j f})*g = (ik_j\hat{f})\hat{g} = ik_j(\hat{f}\hat{g}) = ik_j\widehat{f*g} = \partial_j(\widehat{f*g})$$

This definition comprehends (1.3) if g is chosen as

$$g_\delta(\mathbf{y}) = \frac{1}{V_\delta}\chi_{\mathcal{I}_\delta}(\mathbf{y})$$

where in general χ_A is the characteristic function of the set A, equal to 1 within A and equal to zero otherwise.

From a theoretical point of view it has been considered worthwhile to consider linear average operators that, even if not continuous, have the property of being easily invertible, in order to reconstruct f from its average $< f >$ (Germano (1992)). This lead to the introduction of the so called differential averages, in which the weight function is chosen as the Green function of a given differential operator. In any case, it will turn to be useful to consider how obtain, at least formally, function f from $<f>$. The approach developed here, and which will be used in following discussions, is based on power series developments. The only smoothness requirement is that f, and consequently $<f>$, be analytical. All the calculations will be

carried out for definition (1.3) instead of the more general (1.4), but results may be easily transferred with only few modifications.

The first step is to expand $<f>$ as function of f. With the above hypothesis, we expand the integrand f in (1.3),

$$<f>_\delta (\mathbf{x},t) = \frac{1}{V_1}\int_{\mathcal{I}_1}\sum_{n=0}^{\infty}\frac{\delta^n}{n!}\sum_{k=0}^{n}\sum_{j=0}^{k}\binom{n}{k}\binom{k}{j}\zeta_1^{n-k}\zeta_2^{j}\zeta_3^{n-k}\partial_1^{n-k}\partial_2^{j}\partial_3^{k-j}f(\mathbf{x},t)\mathrm{d}\mathbf{x}. \tag{1.6}$$

If δ is smaller than the radius of convergence of the power series of f, the convergence is then uniform within I_δ and we may perform integration term by term (Rudin (1974)). The result is

$$<f>_\delta (\mathbf{x},t) = \sum_{n=0}^{\infty}\frac{\delta^{2n}}{(2n)!}\sum_{k=0}^{n}\sum_{j=0}^{k}\frac{a_{n-k,j,k-j}}{(2n-2k)!(2j)!(2k-2j)!}\partial_1^{2(n-j)}\partial_2^{j}\partial_3^{2(k-j)}f(\mathbf{x},t) \tag{1.7}$$

where we have defined

$$a_{\alpha,\beta,\gamma} = \frac{1}{V_1}\int_{\mathcal{I}_1}\zeta_1^{2\alpha}\zeta_2^{2\beta}\zeta_3^{2\gamma}\mathrm{d}\boldsymbol{\zeta} \tag{1.8}$$

Owning to the symmetry of $\mathcal{I}_\delta$, coefficients $a_{\alpha,\beta,\gamma}$ are invariants to all permutations of indexes α, β, γ; moreover, they depend only on the shape of the class of sets $\mathcal{I}_\delta$. This expression may be made compact if the following linear differential operators are defined:

$$A_n = \frac{1}{(2n)!}\sum_{k=0}^{n}\sum_{j=0}^{k}\frac{a_{n-k,j,k-j}}{(2n-2k)!(2j)!(2k-2j)!}\partial_1^{2(n-j)}\partial_2^{j}\partial_3^{2(k-j)} \tag{1.9}$$

so that

$$<f>_\delta (\mathbf{x},t) = \sum_{n=0}^{\infty}\delta^{2n}A_n[f(\mathbf{x},t)] \tag{1.10}$$

Our aim is to write f in term of $<f>$ as a power series inverting (1.10). We start writing

$$f(\mathbf{x},t) = \sum_{m=0}^{\infty}\delta^{2m}B_m[<f>_\delta (\mathbf{x})] \tag{1.11}$$

where $\{B_m\}$ is a succession of differential operators to be determined. Then we introduce this expression into (1.10). From the constantness of δ and the commutation of A_m and B_m, employing the regularity property stated for f, we get

$$<f>_\delta = \sum_{n=0}^{\infty} \delta^n \sum_{j=0}^{n} A_{n-j} B_j [<f>_\delta] \tag{1.12}$$

Equating all powers of δ on the left and right hand side the following sequence of operator equations is obtained:

$$A_0 B_0 = I$$
$$\sum_{j=0}^{n} A_{n-j} B_j = 0$$

where I is the identity operator. Observing from (1.9) that $A_0 = I$, we get

$$B_0 = I \tag{1.13}$$
$$B_n = -\sum_{j=0}^{n-1} A_{n-j} B_j \tag{1.14}$$

From (1.9) we have

$$\begin{aligned}
A_1 &= \frac{1}{2} a_{0,0,1} \nabla^2 \\
A_2 &= \frac{1}{8} \left[\frac{a_{0,0,2}}{6} \sum_i \partial_i^4 + a_{0,1,1} \sum_{i \neq j} \partial_i^2 \partial_j^2 \right] \\
A_3 &= \frac{1}{48} \left[\frac{a_{0,0,3}}{90} \sum_i \partial_i^6 + \frac{a_{0,1,2}}{48} \sum_{i \neq j} \partial_i^2 \partial_j^4 + a_{1,1,1} \partial_1^2 \partial_2^2 \partial_3^2 \right] \\
&\dots
\end{aligned}$$

and the first few terms are explicitely given by

$$\begin{aligned}
B_1 &= -A_1 = -\frac{1}{2} a_{0,0,1} \nabla^2 \\
B_2 &= -A_2 + A_1 A_1 = \frac{1}{4} \left[a_{0,0,1}^2 - \frac{a_{0,0,2}}{12} \right] \sum_i \partial_i^4 + \frac{1}{2} \left[a_{0,0,1}^2 - \frac{a_{0,1,1}}{4} \right] \sum_{i \neq j} \partial_i^2 \partial_j^2 \\
B_3 &= -A_3 + 2 A_1 A_2 + A_1^3 = \frac{1}{8} \left[a_{0,0,1}^3 + \frac{1}{6} a_{0,0,1} a_{0,0,2} - \frac{a_{0,0,3}}{540} \right] \sum_i \partial_i^6 + \\
&\quad + \left[\frac{3}{8} a_{0,0,1}^3 + a_{0,0,1} a_{0,1,1} + \frac{1}{6} a_{0,0,1} a_{0,0,2} - \frac{a_{0,1,2}}{36} \right] \sum_{i \neq j} \partial_i^2 \partial_j^4 +
\end{aligned}$$

$$+\frac{1}{8}\left[6a_{0,0,1}^3 + 3a_{0,0,1}a_{0,1,1} - \frac{a_{1,1,1}}{6}\right]\partial_1^2\partial_2^2\partial_3^2$$
$$\dots$$

These properties will be used in the forecoming discussion of sections 2.3 and 2.4.

2. 2 Averaged fields balance equations

Balance equations for averaged flow variables are obtained applying the average operator to balance equation for unfiltered fields, taking advantage from the linearity and commutative properties. Continuity and momentum balance equations give

$$\partial_t <\rho> +\partial_j <\rho u_j> = 0 \tag{1.15}$$
$$\partial_t <\rho u_i> +\partial_j <\rho u_i u_j> = -\partial_i <p> +\partial_j <T_{ij}> \tag{1.16}$$

that for the special case of incompressible homogeneous flows, which we are primary concerned with, take the form

$$\partial_i <u_i> = 0 \tag{1.17}$$
$$\rho(\partial_t <u_i> +\partial_j <u_i u_j>) = -\partial_i <p> +\partial_j <T_{ij}>, \tag{1.18}$$

the latter of which is normally rewritten as

$$\partial_t <u_i> +\partial_j(<u_i><u_j>) = -\rho^{-1}\partial_i <p> +\nu\,\partial_{jj}^2 <u_i> +\partial_j R_{ij}, \tag{1.19}$$

where $R_{ij} =<u_i><u_j> - <u_i u_j>$ are the Reynolds "subgrid" stresses, which represent the effect of momentum flows of scale smaller than δ in the averaged budget. These equations are considered in turbulent flow applications, to evidentiate the greatest scales of the flow. An angular momentum equation arises naturally in a space averaged description, in which the balances on finite dimension systems are considered. The angular momentum of a general mechanical system consists, from the König's theorem, of two contributions, the first one coming from the collective motion of the system as a whole, the second one coming from the internal relative motions of the system. The first one is simply the moment of the momentum of the centre of mass, so that it does not contain any further information, while the latter is computable subtracting from the total angular momentum the moment of first one. With reference to incompressible fluids, the intrinsic angular momentum per unit mass is

$$h_i = \varepsilon_{i\ell k}(<x_\ell u_k> - <x_\ell><u_k>) \tag{1.20}$$

An evolutive equation for h_i may be likewise obtained from momentum equation taking the difference between the average of the angular momentum equation and the momentum of the averaged momentum equation, thus obtaining

$$\partial_t h_i + \partial_j(h_i <u_j>) = \partial_j C_{ij} + \partial_j M_{ij} + \beta_i \tag{1.21}$$

where

$$\begin{aligned} C_{ij} &= \varepsilon_{i\ell k}[(<x_\ell u_k> - <x_\ell><u_k>) <u_j> -(<x_\ell u_k u_j> - <x_\ell><u_k u_j>)] \\ M_{ij} &= \varepsilon_{i\ell k}[<x_\ell T_{kj}> - <x_\ell><T_{kj}>] \end{aligned}$$

Tensor $C_{ij}$is the angular momentum flow due to macroscopic motions, and comprehends either "turbulent transport" due to small scale eddies either the transfer due to the stretching, while M_{ij} is the flow due to molecular transport.

2. 3 Angular momentum and vorticity

We consider the relationship between angular momentum and vorticity and between their balance equations. It is usually assumed that vorticity represents the angular velocity of a small volume of fluid and its balance equation is derived taking the curl of the momentum balance equation. Nigmatulin & Nikolaevskii (1970) and Chatwin (1973) showed the proportionality, at a first order approximation in the square of the linear dimension of a small fluid volume, of vorticity and angular momentum, and then between the vorticity equation and the angular momentum equation.

The limiting assumptions were incompressibility and the use of a first order spatial approximation that may not be appropriate when material elements are considered because of the great deformations which all fluid elements may undergo. We expand the intrinsic angular momentum by means of a power series of the linear dimension δ carried out at the general order m. A result associated to the availability of this infinite expansion is the representation of the balance of the intrinsic momentum as an infinite sequence of differential equations acting on the momentum, the first of which coincides with the vorticity balance, i.e. the Helmoltz equation.

Based on definition (1.3 or 1.4), we define a mean intrinsic moment operator $\mathbf{M}$, acting on a vector field $\mathbf{f}$, as

$$(\mathbf{Mf})_i = \varepsilon_{i\ell k}(< x_\ell f_k > - < x_\ell >< f_k >) \tag{1.22}$$

or also, substituting the explicit definition of the mean,

$$(\mathbf{Mf})_i = \varepsilon_{i\ell k}\frac{1}{V_\delta}\int_{\mathcal{I}_\delta}\eta_\ell f(\mathbf{x}+\boldsymbol{\eta},t)\mathrm{d}\boldsymbol{\eta} \tag{1.23}$$

In the same hypothesis of (1.10), expanding $\mathbf{M}$ in a power series of δ^2 or through substitution of (1.11) into (1.22), we get:

$$\mathbf{M} = \sum_{m=0}^{\infty}\frac{\delta^{2m+2}}{(2m+2)!}\mathbf{C}^{(m)}, \tag{1.24}$$

where

$$C_{ik}^{(m)} = \varepsilon_{i\ell k}\sum_{t=0}^{m}\sum_{j=0}^{t}\binom{2m+1}{2t+1}\binom{2t+1}{2j+1}a_{m-t,t-j,j+1}\partial_\ell^{2j+1}\partial_p^{2(t-j)}\partial_q^{2(m-t)}$$

Coefficients $a_{\alpha,\beta,\gamma}$ are given by (1.8). Here the index p is the integer remainder of $(\ell+1)/3$, while index q is the integer remainder of $(\ell+2)/3$ so that ℓ, p, q are a permutation of 1,2,3. To deduce (1.24) we take advantage of the simmetry of $\mathcal{I}_\delta$.
The mean intrinsic angular momentum per unit mass $\mathbf{h}$ of each element $\mathcal{I}_\delta$ is defined as $<\rho>\,\mathbf{h} = \mathbf{M}(\rho\mathbf{u})$. Relations (1.24) yield to

$$h_i = \frac{1}{2}a_{0,0,1}\varepsilon_{i\ell k}\frac{\partial_\ell(\rho u_k)}{\rho}\delta^2 + \frac{1}{\rho}\left\{-\frac{1}{4}a_{0,0,1}^2\varepsilon_{i\ell k}\partial_\ell(\rho u_k)\frac{\nabla^2\rho}{\rho}+\right.$$
$$\left.+\frac{1}{4!}\left[3a_{0,1,1}\nabla^2\varepsilon_{i\ell k}\partial_\ell(\rho u_k)+(a_{0,0,2}-3a_{0,1,1})\varepsilon_{i\ell k}\partial_\ell^3(\rho u_k)\right]\right\}\delta^4 + O(\delta^6) \tag{1.25}$$

that may be written also in terms of averaged quantities, from (1.11), as

$$h_i = \frac{1}{2}a_{0,0,1}\varepsilon_{i\ell k}\frac{\partial_\ell <\rho><u_k>}{<\rho>}\delta^2 +$$
$$+\frac{1}{<\rho>}\left\{\frac{1}{4!}\left[3(a_{0,1,1}-2a_{0,0,1}^2)\nabla^2\varepsilon_{i\ell k}\partial_\ell(<\rho><u_k>)+\right.\right.$$
$$\left.+(a_{0,0,2}-3a_{0,1,1})\varepsilon_{i\ell k}\partial_\ell^3(<\rho><u_k>)\right]+$$
$$\left.-\frac{1}{4}a_{0,0,1}\varepsilon_{i\ell k}\partial_\ell(\partial_s <\rho>\,\partial_s <u_k>)\right\}\delta^4 + O(\delta^6) \tag{1.26}$$

For compressible flows, the mean intrinsic angular momentum may not be proportional, however small is δ, to the vorticity or to the mean vorticity field, because of the inequal distribution of mass in the volume. The angular

momentum balance equation (1.21) was obtained applying the operator $\mathbf{M}$ to the momentum budget

$$f_k(\mathbf{x},t) = \partial_t(\rho u_k) + \partial_j(\rho u_k u_j) - \partial_j T_{kj} - \rho b_k$$

where $\mathbf{T}$ is the stress tensor and $\mathbf{b}$ is an external force field, and we might expand it term by term, but it is more convenient to apply directly the expansion of operator $\mathbf{M}$ to the momentum budget. Assuming again an analitic behaviour, with positive radius of convergence, for the solutions of the Navier-Stokes equations, and equating to zero all the coefficients of the series (1.24), one gets $\mathbf{C}^{(m)}\mathbf{f} = \mathbf{0}$, $\forall m \in I\!N$, that reduces to

$$\varepsilon_{i\ell k}\,\partial_\ell^{2m+1} f_k(\mathbf{x},t) = 0 \quad \forall m \in I\!N, \quad i = 1,2,3$$

as it can be demonstrated by induction. In fact equations $\mathbf{C}^{(m)}\mathbf{f} = 0$ may be rewritten as

$$(\mathbf{C}^{(m)}\mathbf{f})_i = \sum_{j=0}^{m} \mathcal{D}^{(j)}[\varepsilon_{i\ell k}\partial_\ell^{2j+1} f_k]$$

where $\mathcal{D}^{(j)}$ are linear differential operators, of which $\mathcal{D}^{(j)}$ is the identity operator. Free of any approximation the angular momentum balance leads us to a sequence of differential equations that, by the induction process, are not reducible one to the other, the first of which is the vorticity equation.

The higher order equations are obtained applying the operators $H_{ik}^{(m)} = \varepsilon_{i\ell k}\partial_\ell^{2m+1}$ that show a structure analog to 'higher order' curls and may be considered balances for higher order vorticities. This result is quite general because is not restricted by the particular nature of the constitutive equation as long as this last describes the fluid, even if with internal structure, as a fluid with bulk properties. It might turn useful in turbulence applications where auxiliar equations are always needed as consequence of the introduction of correlation variables associated to the closure of the filtered problem.

2. 4 Variable filter width

In many circustances it is useful to consider a ligthly different average procedure, in which a variable filter width is allowed. This happens when a material boundary on the flow domain is to be taken in account. In fact, even if the centre of the averaging domain lies in the flow domain but its distance to the boundary is less than δ, the averaged field carries an uncorrect information. For example, the averaged velocity is not zero at a rigid

wall. Furthermore, near the boundaries the model employed for nonlinear convective terms is no more valid because turbulent scales are different from far from walls. Then, (1.10) is replaced by

$$<f>(\mathbf{x},t) = \frac{1}{V_1}\int_{\mathcal{I}_1} f(\mathbf{x}+\delta(\mathbf{x})\boldsymbol{\zeta},t)\mathrm{d}\boldsymbol{\eta} \tag{1.27}$$

and (1.4) undergoes analogous modifications. However, when a variable filter width is allowed, one has to face with some additional problems in deriving balance equations for averaged quantities, the most important af which is the lost of the commutability property between filtering and differentiation, which prevents straigthforward application of filtering on equations. This loss of commutability is enterely related to the spatial modulation of a variable filter width.

The problem of the non commutability of the filtering operation has been already considered by Ghosal & Moin (1995) by introducing an alternative definition of the filtering builded on the mapping function of the non uniform grid. Their idea was to transform the physical domain in an unbounded domain on which standard space averaging with constant δ is applied. In this way the commutation error was shown to be of the second order in the maximum filter width. To cope with the commutation error they proposed also the adoption of an asymptotic expansion in the square of the filter width, up to any order of accuracy, where the coefficients of each term depend on the filtered field and its space derivatives. A procedure of this kind would be necessarily adopted in case of numerical schemes based on higher order finite differencing or pseudo-spectral methods. However, to obtain the correction, it requires the solution of additional non homogeneous perturbative problems containing higher orders derivatives of the basic solution. Furthermore, when translated back to physical domain, their procedure define an asymmetric average domain.

We prefer to work directly on physical space without any reference to any numerical discretization scheme. The method we propose is to approximate relationship (1.31). In this way the error is reduced without the need to iteratively solve other equations.

When the filter scale is function of the point, the relation between the space derivative of any filtered physical quantity and the filter of the derivative of the same quantity is

$$\frac{\partial}{\partial x_i} < f >_\delta \;=\; \frac{1}{V_1}\int_{\mathcal{I}_1} \frac{\partial f}{\partial x_i}(\mathbf{x}+\delta(\mathbf{x})\boldsymbol{\zeta})\mathrm{d}\boldsymbol{\zeta} + \tag{1.28}$$

$$
\begin{aligned}
+ \quad & \frac{\partial \delta}{\partial x_i}(\mathbf{x}) \frac{1}{V_1} \int_{\mathcal{I}_1} \frac{\partial f}{\partial x_j}(\mathbf{x} + \delta(\mathbf{x})\boldsymbol{\zeta})\zeta_j \mathrm{d}\boldsymbol{\zeta} = \\
= \quad & < \frac{\partial f}{\partial x_i} >_\delta + \frac{\partial \delta}{\partial x_i} < \nabla_{\mathbf{x}} f \cdot \boldsymbol{\zeta} >_\delta
\end{aligned} \tag{1.29}
$$

This relationship may be contracted if one ascertains that

$$
\frac{\partial}{\partial \delta} < f >_\delta = \frac{1}{V_1} \int_{\mathcal{I}_1} \frac{\partial f}{\partial x_j}(\mathbf{x} + \delta(\mathbf{x})\boldsymbol{\zeta})\zeta_j d\boldsymbol{\zeta} \tag{1.30}
$$

The result is a relation where the filter of the derivative is a differential operator acting on the filtered field:

$$
< \frac{\partial f}{\partial x_i} >_\delta = \frac{\partial}{\partial x_i} < f >_\delta - \frac{\partial \delta}{\partial x_i} \frac{\partial}{\partial \delta} < f >_\delta \tag{1.31}
$$

As a first attempt, this problem could be faced adopting a truncated series expansion of $< f >_\delta$ in terms of powers of δ. In fact, from (1.10), we can write

$$
\frac{\partial}{\partial \delta} <f> = 2\delta A_1[f] + 4\delta^3 A_2[f] + O(\delta^5)
$$

up to the desidered order of accuracy, with operators A_i specified by (1.9). The following step is to write substitute the expansion of f in terms of $<f>$. Special attention must be reserved in using expression (1.11), which was deducted in the hypothesis of constant δ. Anyway, the first order is not affected by this problem and it is easily found

$$
\frac{\partial}{\partial \delta} <f> = 2\delta A_1[<f>] + O(\delta^3) \tag{1.32}
$$

Introducing (1.32) into (1.31) and substituting $\delta(\mathbf{x}) = \Delta\phi(\mathbf{x})$ one would recover the result by Ghosal & Moin (1995) about second order error when non commutability is neglected and furthermore has a procedure to approximate it. Even if this might be extended to any order of accuracy, it present the disvantage of increasing the order of the equations, requiring consequently additional boundary conditions. We proposed then a different treatment based on numerical approximation of the δ-first derivative in conjunction with truncated expansions. Let us write the second order finite difference approximation

$$
\frac{\partial < f >_\delta}{\partial \delta} = \frac{1}{2h} \left(< f >_{\delta+h} - < f >_{\delta-h} \right) + O(h^2) \tag{1.33}
$$

We choose $h = \delta$ and express $< f >_{2\delta}$ and $< f >_0 = f$ in terms of $< f >_\delta$. By means of (1.10) we have

$$f =< f >_\delta - \frac{1}{2} a_{0,0,1} \delta^2 \nabla^2 f + O(\delta^4)$$

Averaging again on a volume of linear dimensions 2δ, and observing from (1.10) and (1.11) that the difference between $< \delta^2 \nabla^2 f >_{2\delta}$ and $\delta^2 \nabla^2 f$ is $O(\delta^4)$, we obtain

$$< f >_{2\delta} =<< f >_\delta >_{2\delta} - a_{0,0,1} \delta^2 \nabla^2 f + O(\delta^4)$$

Introducing $< f >_{2\delta}$ and f in (1.33), we finally get

$$\frac{\partial < f >_\delta}{\partial \delta} = \frac{1}{2\delta} (<< f >_\delta >_{2\delta} - < f >_\delta) + O(\delta^2) \equiv H_\delta(< f >) + O(\delta^2). \tag{1.34}$$

When approximation (1.34) is used, equation (1.31) will be affected by a third order error. This procedure should then turn useful in numerical computations with at least a third order numerical scheme when integrating the resulting equations. In the equation of (1.19) this leads to the substitution of $\partial_j R_{ij}$ with

$$\partial_j R_{ij} + (\partial_j \delta) H_\delta(< u_i >< u_j > - R_{ij})$$

and of $\partial_i < p >$ with $\partial_i < p > - (\partial_i \delta) H_\delta(< p >)$. In an analogous way additional terms in the angular momentum equation (1.21) are introduced. An approximation of the error on order second derivatives is also needed.

3. Structured flows

3. 1 Granular flows

A major system in which the angular momentum balance comes strongly and indipendently into the dynamics is the case of granular flows. A granular flow may be regarded as the motion of an heterogeneous medium of the type gas-solid particles, without phase transition, when the phase density ratio has the limiting value of zero. Examples are the rapid motion of ice grains freely flying between successive binary collisions met in planetary rings, see for instance Araki & Tremaine (1986), Wisdom & Tremaine (1988), Frezzotti (1998), and fluidized regimes of rough particles, see Cercignani & Lampis (1988), Goldshtein & Shapiro (1995).

The starting point is a kinetic model, first developed by Enskog in the context of dense gases. In the classical Boltzmann theory, the assumption of

negligible small molecular volume in comparison with the volume occupied by the whole gas is made. With this Ansatz molecules are consequently considered as material points and have then only translational degrees of freedom. In granular systems this assumption is abandoned, and it is necessary to introduce new variables which describe the internal degrees of freedom. The simplest case is that of rigid spheres whose mass center coincides with the geometrical centre and whose inertia momenta tensor is isotropic. This representation owns the advantage that no variable is explicitly required to specify the orientation of grains in space, and so only three vector variables, namely the position $\mathbf{x}$ of the centre, the velocity $\mathbf{u}$ of the centre and the angular velocity $\mathbf{\Omega}$, are sufficient the dynamical status of each grain. Interaction between grains are limited to binary collisions. Three are the fundamental differences with the kinetic theory by Boltzmann, primary due to finite dimensions of grains: the centre of the molecules are not assumed to coincide at a collision, but they are at a distance of a sphere diameter; although multiple collisions are not considered, the closeness of other molecules produces a modification in the collision rate, such that the two-particle distribution function is no more equal to the product of one -particle distribution. Finally, inelasticity and roughness of grains are considered in collisions.

These hypothesis led to the Enskog's equation for the particle distribution function $f(t, \mathbf{x}, \mathbf{u}, \mathbf{\Omega})$ that probabilistically describes the collective motion (Cercignani & Lampis (1988)),

$$\frac{\partial f}{\partial t} + u_j \frac{\partial f}{\partial x_j} + \frac{F_j}{m}\frac{\partial f}{\partial u_j} + \frac{M_j}{I}\frac{\partial f}{\partial \Omega_j} = J_E(f, f) \tag{1.35}$$

where m and I are mass and momentum of inertia of grain while F_j and M_j are the external force and momentum acting on them. The collision operator J_E is defined as (Cercignani & Lampis (1988), Goldshtein & Shapiro (1995))

$$J_E(f,f) = a^2 \int \Theta(\boldsymbol{\varepsilon}\cdot\mathbf{u}_{12})[g_2(\mathbf{x}, \mathbf{x}-a\boldsymbol{\varepsilon}) f(\mathbf{x}, \mathbf{u}^*, \mathbf{\Omega}^*, t) f(\mathbf{x}-a\boldsymbol{\varepsilon}, \mathbf{u}_2^*, \mathbf{\Omega}_2^*, t)$$
$$-g_2(\mathbf{x}, \mathbf{x}+a\boldsymbol{\varepsilon}) f(\mathbf{x}, \mathbf{u}_1, \mathbf{\Omega}, t) f(\mathbf{x}+a\boldsymbol{\varepsilon}, \mathbf{u}_2, \mathbf{\Omega}_2, t)](\boldsymbol{\varepsilon}\cdot\mathbf{u}_{12})\mathrm{d}\mathbf{u}_2\mathrm{d}\Omega_2\mathrm{d}^2\boldsymbol{\varepsilon}. \tag{1.36}$$

Here Θ is the Heaviside function, g_2 is the equilibrium pair correlation function, whose expression may be read in Cercignani & Lampis (1988), $\boldsymbol{\varepsilon}$ is the versor of the direction connecting the centres of the two colliding grains, $\mathbf{u}_{12} = \mathbf{u}_1 - \mathbf{u}_2$ and variables with a star are the initial velocities and angular velocities leading to final velocities and angular velocities $\mathbf{u}$, $\mathbf{\Omega}$, $\mathbf{u}_2$, $\mathbf{\Omega}_2$ after

the collision. They are obtained from the collision relations, which are obtained from the conservation of momentum and angular momentum in each collision the collision model (Frezzotti (1998))

$$\mathbf{u}_R = -e(\boldsymbol{\varepsilon}\cdot\mathbf{u}_R^*)\boldsymbol{\varepsilon} - \beta(\mathbf{u} - (\boldsymbol{\varepsilon}\cdot\mathbf{u}_R^*)\boldsymbol{\varepsilon}),$$

where $\mathbf{u}_R$ is the relative velocity in the impact point and e and β are the restitution and roughness factors; they take the form (Frezzotti (1998))

$$\begin{aligned}
\mathbf{u} &= \mathbf{u} + \frac{1+e}{2}(\boldsymbol{\varepsilon}\cdot\mathbf{u}_R^*)\boldsymbol{\varepsilon} + \frac{k(1+\beta)}{2(1+k)}(\mathbf{u} - (\boldsymbol{\varepsilon}\cdot\mathbf{u}_R^*)\boldsymbol{\varepsilon}) \\
\mathbf{u}_2 &= \mathbf{u} + \frac{1+e}{2}(\boldsymbol{\varepsilon}\cdot\mathbf{u}_R^*)\boldsymbol{\varepsilon} + \frac{k(1+\beta)}{2(1+k)}(\mathbf{u} - (\boldsymbol{\varepsilon}\cdot\mathbf{u}_R^*)\boldsymbol{\varepsilon}) \\
\boldsymbol{\Omega} &= \boldsymbol{\Omega} - \frac{1+\beta}{a(1+k)}(\boldsymbol{\varepsilon}\wedge\mathbf{u}_R^*) \\
\boldsymbol{\Omega}_2 &= \boldsymbol{\Omega}_2 - \frac{1+\beta}{a(1+k)}(\boldsymbol{\varepsilon}\wedge\mathbf{u}_R^*)
\end{aligned}$$

where $k = 4J/a^2$. Parameter e affects only the final normal velocities, while parameter β affects tangential velocities and angular velocities. Value of $e = 1$ corresponds to elastic collisions while $\beta = -1$ correspond to smooth collisions with no angular velocity exchange.

Macroscopic field variables are straightforward defined as

$$\overline{\varphi} = \frac{\int \varphi f \mathrm{d}\mathbf{u}\mathrm{d}\boldsymbol{\Omega}}{\int f \mathrm{d}\mathbf{u}\mathrm{d}\boldsymbol{\Omega}}$$

where the denominator is the numerical density n of particles. Balance equations for granular flows are obtained multiplying the Enskog equation (1.35) for the physical quantity φ and averaging

$$\frac{\partial}{\partial t}(n\overline{\varphi}) + \frac{\partial}{\partial x_j}(n\overline{\varphi u_j}) = \overline{f u_j \frac{\partial \varphi}{\partial x_j}} + \overline{f F_j \frac{\partial \varphi}{\partial u_j}} + \overline{f M_j \frac{\partial \varphi}{\partial \Omega_j}} + n\Delta\varphi \qquad (1.37)$$

where

$$n\Delta\varphi = \int \varphi J_E(f,f)\mathrm{d}\mathbf{u}\mathrm{d}\boldsymbol{\Omega}$$

The most interesting result is that, even if φ is a collisional invariant, that is a quantity that is conserved in collisions, and thus satisfies

$$\varphi(\mathbf{u}_2', \boldsymbol{\Omega}_2') - \varphi(\mathbf{u}_2, \boldsymbol{\Omega}_2) = -[\varphi(\mathbf{u}', \boldsymbol{\Omega}') - \varphi(\mathbf{u}, \boldsymbol{\Omega})]$$

(collisional invariants are mass, momentum and total angular momentum), $n\Delta\varphi$ is not zero if φ is not constant. This implies that, except the continuity equation, which remains unchanged, the momentum and angular momentum equations will contain additional flow contributions arising from interactions at distance due to the finite dimensions of the colliding grains. The momentum balance equation is obtained putting $\varphi = mu_i$; the stress tensor is now found to be $T_{ij} = T^k_{ij} + T^c_{ij}$, where (Cercignani & Lampis (1988))

$$\begin{aligned} T^k_{ij} &= -m\int (u_i - \overline{u}_i)(u_j - \overline{u}_j) f \mathrm{d}\mathbf{u}\mathrm{d}\Omega \\ T^c_{ij} &= \frac{ma^2}{2}\int\!\!\int_0^a (u_i - u_i^*)\varepsilon_j \Theta(\boldsymbol{\varepsilon}\cdot\mathbf{u}_{12}) g_2(\mathbf{x} + (\alpha - a)\boldsymbol{\varepsilon}, \mathbf{x}) \\ &\times \; f(\mathbf{x} + (\alpha - a)\boldsymbol{\varepsilon}, \mathbf{u}, \boldsymbol{\Omega}) f(\mathbf{x} + \alpha\boldsymbol{\varepsilon}, \mathbf{u}_2, \boldsymbol{\Omega}_2) \mathrm{d}\alpha\mathrm{d}\mathbf{u}\mathrm{d}\boldsymbol{\Omega}\mathrm{d}\mathbf{u}_2\mathrm{d}\boldsymbol{\Omega}_2. \end{aligned}$$

Here superscript k denotes the "kinetic" contribution and superscript c denotes the collisional contribution. One of the most relevant feature is that now T^c_{ij} is not symmetric in general unless spheres are smooth, in which case collisions affect only the normal component of the relative velocity.

When the same reasoning is applied to the total angular momentum, that is $\varphi = \varepsilon_{i\ell k} x_\ell u_k + mJ\Omega_i$, we have equation

$$\partial_t(\rho J\overline{\Omega}_i) + \partial_j(\rho J\overline{\Omega}_i\overline{u}_j) = \rho\beta_i + \varepsilon_{ijk}T^c_{jk} + +\partial_j K_{ij} \tag{1.38}$$

after having subtracted the moment of momentum equation, where $\overline{\boldsymbol{\Omega}}$ is the mean angular velocity of the grains and $K_{ij} = K^k_{ij} + K^c_{ij}$ the angular momentum flow, given by

$$\begin{aligned} K^k_{ij} &= -mJ\int \Omega_i(u_j - \overline{u}_j) f \mathrm{d}\mathbf{u}\mathrm{d}\boldsymbol{\Omega} \\ K^c_{ij} &= -\frac{ma^2}{2}\int\!\!\int_0^a \varepsilon_i\varepsilon_{j\ell k}[(\alpha - a)\varepsilon_\ell(u_j - u_j^*) + J(\Omega_j - \Omega_j^*)](\boldsymbol{\varepsilon}\cdot\mathbf{u}_{12}) \\ &\times \; \Theta(\boldsymbol{\varepsilon}\cdot\mathbf{u}_{12}) g_2(\mathbf{x} + (\alpha - a)\boldsymbol{\varepsilon}, \mathbf{x}) f(\mathbf{x} + (\alpha - a)\boldsymbol{\varepsilon}, \mathbf{u}, \boldsymbol{\Omega}) \\ &\times \; f(\mathbf{x} + \alpha\boldsymbol{\varepsilon}, \mathbf{u}_2, \boldsymbol{\Omega}_2) \mathrm{d}\alpha\mathrm{d}\mathbf{u}\mathrm{d}\boldsymbol{\Omega}\mathrm{d}\mathbf{u}_2\mathrm{d}\boldsymbol{\Omega}_2. \end{aligned}$$

In this way momentum and angular momentum are naturally coupled, because rough collisions are non central interactions at distance that couples the changes of velocity and angular velocity.

This would be clearly visible if constitutive equations were developed. Even if the existence of an hydrodynamic stage for the evolution of granular systems is not proved, approximate moment methods (Araki & Tremaine

(1986)) and Chapman-Enskog expansions (Goldshtein & Shapiro (1995)) have been used to derive them, resulting in a different evaluation of the partition of the kinetic energy between rotational and translational modes. Goldshtein & Shapiro (1995) have shown that inelasticity has the capability to shift the partition of the kinetic energy in favour of the rotational modes. The particle spin is an important feature of the distribution function and it must not be generally neglected when deriving the evolutive equations at the macroscopic level. When grains are rough and extended, or when the interaction among grains is not only limited to collisions because of the presence of long range gravitational interaction or externally imposed forces and torques, the difference between instantaneous and mean particles spins must be accounted for. For simplicity the average spin was always assumed equal to the mean vorticity by both Araki & Tremaine (1986) and Goldshtein & Shapiro (1995). This may not be exactly true. It has been found a relative difference between mean angular spin and average vorticity of about 70% both in Salo (1995), by means of the molecular dynamics of grains in presence of the mutual gravitational interaction, and in Frezzotti (1998), through linearized Enskog theory applied to rough and inelastic elements. The leading order of equations obtained from the Chapman-Enskog expansion is constituted by non-diffusive Euler-like equations, while in the second order the distribution function is a quasi-linear function of the hydrodynamic dependent variables, that in the general case comprehend also $\overline{\boldsymbol{\Omega}}$. As a consequence, at this order, the angular momentum balance results explicitely coupled to the balance of mass, momentum and energy. Instead at the first order (Euler-like equations) the diffusive flow is zero and the mean particle spin $\overline{\Omega}_i$ remains constant on each particle path. In both cases it cannot be replaced by the vorticity of the mean flow which undergo a different dynamics, as it is remarked by the absence in (1.38) of a stretching term even in tridimensional configurations of motion.

3. 2 Biphase flows

When dealing with suspensions the main purpose is the description of global large-scale behaviour. Different ways were proposed, depending on the particular problem and on the goal of the analysis.

When the density ratio between the two phases is equal or near to unity, it is possible to macroscopically describe the system as an homogenous equivalent fictitious continuum. Batchelor (1970) and Brenner (1970) deduce the system of equations governing the averaged field variables relevant to each phase. A second approach adopts a continuum mechanics point of view

for the global system introducing *ad hoc* postulates that should reproduce the key features of the influence of the dispersed phase on the whole system (for example, see Almog & Brenner (1999), Dahler & Scriven (1963), Eringen (1966) and Ungarisch (1999)). In this case, no explicit average is performed, and the variables are supposed to represent quanties averaged on a somewhat smaller scale (micropolar element, see for instance Eringen, 1966). The aim of both methods is then to fit the global mechanics of the biphase system in an hypothetical fictitious equivalent medium.

A suspension is a system which is defined essentially in a statistical sense inasmuch as the exact location and velocity of the particles is different for different realizations of the same macroscopic conditions. The natural approach is based on ensemble averages, in a way similar to that employed for granular flows, with the major difference that interactions between suspended elements are not due to collisions but to the hydrodynamic interaction with the surrounding fluid flow. Ensemble averages are not easy to be obtained or observed, so it is necessary to consider other average procedures, like the volume averages discussed in section 2.1. This leads to same results under the assumption that the suspension is locally statistically homogeneous Batchelor (1970). The angular momentum balance comes into the analysis of the dynamics of suspensions in presence of external forces and couples acting selectively on the suspended particles. The contribution of the dispersed phase on the volume averaged momentum flow tensor is:

$$\frac{1}{V}\int_{V_0}\sigma_{ij}\mathrm{d}\mathbf{x} = \frac{1}{V}\int_{\partial V_0}\sigma_{ik}x_j n_k \mathrm{d}\sigma - \frac{1}{V}\int_{V_0} x_j\partial_k\sigma_{ik}\mathrm{d}\mathbf{x},$$

with $V_0 = \bigcup_\alpha V_\alpha$, where V_α is the volume occupied by each particle, and the first term on the right hand side is the moment exerted by the fluid on the suspended particles. If each particle is assumed to behave like a dipole due to the presence of a body-force field acting selectively only on the particle and one subtracts from the stress tensor an equivalent hydrostatic field, capable to balance the external body-force (Batchelor, 1970), one would find:

$$\rho a_j = \partial_i\sigma_{ij},$$

where a_j is the local acceleration relative to the averaged global one, and

$$\varepsilon_{ijk}\int_{\partial V_\alpha}\rho a_j x_k \mathrm{d}\sigma - \varepsilon_{ijk}\int_{\partial V_\alpha}\sigma_{jl}x_k n_\ell \mathrm{d}\sigma = \beta_i^\alpha = \varepsilon_{ijk}\int_{V_\alpha}\sigma_{ij}\mathrm{d}\mathbf{x}$$

When substituted back in the momentum flow equation, the excess external moment M_i^α leads to a skew-symmetric part of the momentum flow Σ_{ij} equal

to the mean external angular moment per unit volume, $\varepsilon_{ijk}\Sigma_{jk} = \sum_\alpha \beta_i^\alpha / V$, that will depend also on the particle concentration and orientation. Externally imposed couples on particles might be caused by electric or magnetic fields on particles of ferromagnetic alloys. Batchelor (1970) then develops "constitutive equations" for suspensions in the hypothesis of equal density of the two phases and low concentration, a case in which it is possible to compute an estimate of the moment flow due to particle motions, that would lead, in the case of force-free and torque-free spheres, to Einstein's formula. Similar results are presented also by Brenner (1970).

3. 3 Micropolar flows

A continuum theory in which angular momentum has a central role is that of the so called "micropolar fluids" by Eringen (1966) or of the equivalent "structured continua" by Dahler & Scriven (1963). These authors rely on the idea that "fluid points contained in a small volume element may have a motion different by that of the centroid of the volume element"[2] in which they are embedded, and in particular they may rotate around it. In this theory the fluid medium is depicted as a dense collection of simple material systems, the microelelements, owning momentum, intrinsic angular momentum and energy. The kinematics of the motion of each microelemnt is fully described by the velocity $u_i(\mathbf{x}, t)$ of its centroid and by a second order tensor $\nu_{ij}(\mathbf{x}, t)$, called by Eringen microgyration tensor, which portraits the internal deformation and rotation of the element. In the most simple version of this model, this tensor is skew-symmetric, thus leading to a collective motion of pure rotation of each element. It is supposed that "certain anisotropic fluids, liquid crystals made up of dumbell molecules", "animal blood" and "certain polymeric fluids and fluids containing certain additives may be represented by the mathematical model underlying micropolar fluids"[3]. In this way, this idea leads to the existence of an intrinsic angular momentum field $h_i = \varepsilon_{imn} i_{mp} \nu_{pn}$, where i_{mp} is the microinertia tensor, related to the geometrical properties of the microelements, representing the dynamical effects of the micropolar elements motion. The introduction of this tensor implies a non trivial balance equation for the intrinsic angular momentum which is directly coupled to the linear momentum balance through the onset of a new skew-symmetric part of the macroscopic stress tensor. The momentum and intrinsic angular momentum balance equations may be written, see for

[2] See Eringen, 1966, pag.1.
[3] *ibidem*, pag.1.

example Łukaszewicz (1999), as

$$\rho(\partial_t u_i + u_j \partial_j u_i) = \partial_j T_{ij} + \rho b_i \quad (1.39)$$

$$\rho(\partial_t h_i + u_j \partial_j h_i) = \varepsilon_{ijk} T_{jk} + \partial_j K_{ij} + \beta_i \quad (1.40)$$

where h_i is the intrinsic angular momentum, β_i the mean torque per unit volume, T_{ij} and K_{ij} are the now non-symmetric tensors of the flow of momentum and angular momentum. Equation (1.40) is obtained in the same way as (1.2) is derived from (1.1), only balance (1.1) is now substituted by

$$\frac{\mathrm{d}}{\mathrm{d}t}\int_{A(t)} (\varepsilon_{ijk} x_j \rho u_k + \rho h_i)\mathrm{d}\mathbf{x} =$$

$$= \int_{\partial A(t)} (\varepsilon_{ijk} x_j T_{km} n_m + K_{ij} n_j)\mathrm{d}\sigma + \int_{A(t)} (\varepsilon_{ijk} x_j \rho b_k + \beta_i)\mathrm{d}\mathbf{x} \quad (1.41)$$

Referring to applications to suspensions, it was recently recognized that the asymmetric stress tensor implied by (1.40) has normally no counterpart in an equivalent averaging approach (Almog & Brenner (1999)), even if it is a quite natural result of a postulated continuum approach for the averaged equivalent monophase continuum.

The intrinsic angular momentum is an extensive quantity, linked to the spatial extention of material systems, and vanishes when the dimension of the system reduces to zero. In this model the properties of finite size elements, containing fluid and particles, are then associated to discretized entities (the micropolar local elements) deprived of finite dimensions. This introduces, in our opinion, the main difficulty of the model because the properties of the micropolar elements are not obtained through a limiting process with regard to the ratio between their characteristic linear dimension and a macroscale length. This is a central feature for the possible application of this model. Almog & Brenner (1999) wrote: "the necessity of an antisymmetric stress arises from the fact that the couple generated by a symmetric stress tensor acting over a surface bounding an arbitrary (small) volume vanishes identically", however this happens only when the stress components are forced to act on a same point because the volume has been considered infinitesimal.

Most applications of the micropolar fluid model deal with the mathematical properties of equations (1.39-1.40) with linear constitutive equations for tensors T_{ij} and K_{ij} in terms of gradients of velocity and angular momentum, or tend to solve them on standard situations, like pipe flows, boundary flows and so on to remark differences with the corresponding solutions of the Navier-Stokes equations. Notwithstanding many of the authors think

to suspensions as the natural application, and Brenner (1970), Almog & Brenner (1999) try to match the two situations, it is evident, either from its formulation or from the resulting equations, that it might be well suited not for systems constituted by fluids "containing structures" (solutions) but for fluids constituted by "structures" on a subcontinuum scale, such as granular flows, that might be the most natural application. In effect Dahler & Scriven (1963), Condiff & Dahler (1964) explicitely wrote that micropolar effects arise in the presence of extended subcontinuum entities with non central interactions, and as example stated dense gases.

The comparison by Tözeren & Skalak (1977) between semiempirical models for wall flows calibrated on experimental results enlightens the difficulties of this kind of model in reproducing simple shear flows of a dilute suspension of rigid spheres in water (with $\alpha = 1$). Notwithstanding the flexibility given by the different boundary conditions that may be associated to the micropolar model equations, this last was found not able to reproduce at the same time both particle rotations and mean velocity near the wall for a Couette flow of a dilute suspension of rigid spheres. The disagreement may be referred to the impossibility for the micropolar model to account for variations of the suspension properties due to the concentration variations, a field variable that is completely absent in this theory.

4. Angular momentum past applications in turbulence

4. 1 Early applications of angular momentum in turbulence by Mattioli

Space averaged equations were used from the very beginning in the analysis of turbulent flows, starting from the early works by Reynolds (1895), even if he did not pose himself the problem of closure neither attempted to solve them. Even if intensive use of spatial filtering begins with large eddy simulation with Smagorinsky (1963) and became a standard tool for turbulent flow simulations many years later, balances over finite volumes to evidence the larger scales of turbulence where already considered by many authors (Mattioli (1933), Nigmatulin & Nikolaevsky (1970), Ferrari (1972), Eringen (1972)).

In connection with this approach, it was felt worthwhile to consider the angular momentum of the fluid volume in which averages were taken.

Since the earliest Mattioli's application in 1933, the equation of angular momentum balance has been applied few times to discuss the behaviour of turbulent flows. The approaches then differentiated.

Anyhow, the key point of these theories is the coupling between the

momentum and the moment of momentum equations. In all of them the distribution of the mean velocities depends upon the motion of internal rotation, considered as the structural property of the elemental volume cells. The mathematical coupling between the two kinematical aspects is due to the presence of the antisymmetric part of the turbulent stress tensor in both the equations of momentum and angular momentum.

This feature is explicitly declared in Mattioli, it has been renewed by Ferrari and Nicolaevskii, but it is also a necessary element in the model by Eringen. All these theories seem capable to reproduce experimental results about turbulent sheared flows. In spite of this, their common and decisive component - the coupling between the momentum and angular momentum equations through an antisymmetric part of the stress tensor - is an arbitrary choice, whose validity in the case of homogenous fluid may be proved false.

The first of these works that use angular momentum in turbulence applications are those by Mattioli (1933, 1937), who considered balances over finite fluid elements, and introduced the possibility of a non symmetric stress tensor. His fundamental idea is to deduce from the principles of mechanics the equations for the largest scales of turbulence, if only one relinquishes to describe the details of the fluid motion, likewise to the approach of classical continuum mechanics, in which molecular motions are not considered; field variables that macroscopically describe the collective motion are introduced and balance equations for them are derived directly from general principles of physics.

In this end, he introduces, apart from density and velocity, an additional vector field **h** apt to represent the intrinsic angular momentum of each volume. Then, he founds, other than the continuity equation, equations

$$\mathrm{D}_t < u_i > = \partial_j T_{ij} + \partial_j \tau^a_{ij} + \partial_j \tau^s_{ij} \tag{1.42}$$

$$\mathrm{D}_t h_i = \varepsilon_{ijk}\tau^a_{jk} + \partial_j C_{ij} + \partial_j K_{ij}, \tag{1.43}$$

the second of which is obtained in the same way as (1.2) when in (1.1) $\varepsilon_{i\ell k}x_\ell \rho u_k$ is replaced by $\varepsilon_{i\ell k}x_\ell \rho u_k + \rho h_i$. Here τ_{ij} is the flow of momentum due to smaller scale turbulent fluctuations, which in (1.42-1.43) is decomposed in its symmetric and antisymmetric parts for sake of clearness, and analogously K_{ij} and C_{ij} are the angular momentum flows due to molecular and turbulent transport. The most evident feature of its set of equations is the presence of τ^a_{ij}, on which were addressed the criticism of its contemporary. However, he does not suppose, a priori, that the flow of momentum is not symmetric, but he "deduces" this property from equation (1.43). In fact, being in general h_i not constant, unlike (1.2), $\varepsilon_{i\ell k}\tau^a_{\ell k}$ cannot be zero.

Correctly deduced equation for angular momentum (1.21), starting from the Navier-Stokes equations, does not contain a such term.

The incongruence of its conclusion and of the derivation of (1.43) lies his assumptions on angular momentum balance, where he treats as point entity with spatial extension.

In Mattioli's theory the antisymmetric part of the turbulent stress is assumed and interpreted as the momentum transport due to the vortical structures of the small scales filtered out from the equation. A model is then needed for this term. At this point, closure assumptions on τ_{ij} and C_{ij} are introduced, primary based on modified Boussinesq hypothesis. He also assume, not quite legitimately since dedicating an equation to it, that the intrinsic angular momentum be proportional to the vorticity. With this Ansatz equation (1.43) becomes thus an equation operating on vorticity, but with a different structure than the original Helmoltz equation, because of the presence of the term $\varepsilon_{i\ell k}\tau^a_{\ell k}$ instead of the stretching term. In this way one dependent variable is dropped out, and the additional equation is eventually used as equation for the turbulent transport coefficient.

Mattioli's theory was revised by Ferrari (1972), who justified and extended it on a phenomenological basis.

4. 2 Nikolaevsky's model

To a set of equations very similar to (1.42-1.43) arrived also Nikolaevsky averaging the Navier-Stokes equations. He considered the balances of mass, momentum, angular momentum and energy.

Nikolaevsky (1970) while computing the mean of the derivative introduces an approximation of the second order in δ that induces the lost of the commutative property between derivatives and filtering and consequently of the property of symmetry of the averaged equation, where he obtains the divergence of asymmetric tensors. In fact he uses the Gauss theorem to transform the integral of the divergence in a surface integral. Then in relation to the cubic volumes adopted for averages he approximates incremental ratios with derivatives:

$$<\partial_i f>_\delta (\mathbf{x}, t) = \partial_i [f]_{(i)}(\mathbf{x}, t) + O(\delta^2) \tag{1.44}$$

where one must not sum up over the index in parenthesis and $[f]_{(i)}$ is defined by

$$[f]_{(i)} = (2\delta)^{-2} \int_{-\delta}^{\delta}\int_{-\delta}^{\delta} f(\mathbf{x} + \eta_j \mathbf{e}_j + \eta_k \mathbf{e}_k)\, \mathrm{d}\eta_j\, \mathrm{d}\eta_k, \quad j, k \neq i$$

as the average of f on a plane whose normal lies in the i-direction. Nikolaevsky neglects the terms $O(\delta^2)$. So doing, together with the commutability, he looses the symmetry of the tensors involved in the equations. In this way Reynolds subgrid stresses are now

$$R_{ij} = <u_i><u_j> - [u_i u_j]_{(j)}$$

instead of (1.19) and own an antisymmetric part given by

$$R^a_{ij} = \frac{1}{2}([u_i u_j]_{(i)} - [u_i u_j]_{(j)})$$

that links the equations of momentum and angular momentum. However, it it easy to see that it is of order $O(\delta^2)$ and arises enterely from approximation (1.44).

4. 3 Application of Eringen's micropolar fluid model

In this context of applications of angular momentum balance in the analysis of turbulent flows we have to recall the applications of the general microfluid theory to turbulence, by Eringen (1972). Here the turbulent flows are considered simple microfluids independently from the presence of any physical effect causing asymmetry. Since the microfuid theory already implies a volume averaged form of the equations, no further averaging is applied, and microelements of Eringen's theory (see chapter 1, §3.3) are identifyed with small scale eddies. The motion of each micropolar element is then described not only by the mean velocity $u_i(\mathbf{x}, t)$ but also by the microgyration tensor $\nu_{ij}(\mathbf{x}, t)$, that arise from the collective motion of deformation (its symmetric part) and rotation (its skew-symmetric part) of the small scale eddies represented by each microelement. The resulting system of equations is not reducible to the filtered Navier-Stokes equations and, when linear constitutive relations are introduced, comprehends up to twenty-three coefficients. The intrinsic moment of momentum equation is coupled to the momentum budget by the antisymmetric part of the stress tensor as in Mattioli and Nikolaevsky. It may be seen that if the constrain of zero antisymmetric part of the momentum flow tensor is used in his constitutive equations, the equations result uncoupled, leading to a mean velocity field independent from the internal motions of the microelements described by tensor $\nu_{ij}(\mathbf{x}, t)$.

The wide number of physical coefficients that this model introduces both in the momentum and microgiration balances (1.39 and 1.40) by the linear costitutive equations of this theory allows a flexibility sufficient to comply

with the gross feature of the two-dymensional turbulent channel flow investigated (Eringen (1972)).

In the application to the two dimensional turbulent channel flow Eringen gives a solution of his equations and the constant coefficients, which are now only five thanks to the simple domain geometry, are adjusted according to the experimental observation by Laufer (1951).

Furthermore, in a rather obscure way, a posteriori turbulent Reynolds stresses are symmetric and identified as the average on a microelement of the product of velocity fluctuations to respect to the microelement velocity and then computed, coherently with the micropolar model kinematics, as

$$\tau_{kl} \equiv -\rho\overline{u_i' u_j'} = i_{mn}\nu_{km}\nu_{ln}$$

where i_{mn} is the microinertia tensor and ν_{ij} is the skew-symmetric giration tensor, defined in §3.3. However, this expression is different from that used in the equations that are actually solved .

Chapter 2

Angular momentum large eddy model

1. Angular momentum Les model

From the discussion of previous chapter, it appears that equations coming from spatial averaging of the Navier-Stokes equations always own symmetric flow tensors and that angular momentum equation is not directly coupled to the momentum equation. Applications of models and theories conceived for structured flow to turbulence is then not justified. However, we shall show that the behaviour of intrinsic angular momentum might be of interest in the analysis of turbulent flows, and a large-eddy model based on it will be proposed. This model will finally put forward a different coupling, that does not require any asymmetry of turbulent flow tensors. Even if the presentation will be focused on turbulent incompressible flows, it might be useful also for structured flows (see chapter 1, §2), where an intrinsic angular momentum arises and is coupled with the momentum balance equation.

We employ the Kolmogorov theory to evaluate the order of magnitude of the angular momentum in the case of isotropic homogeneous turbulence. We may write

$$h \sim \delta^{-3} \int_0^{\delta} r(\delta u)_r r^2 \mathrm{d}r$$

where $(\delta u)_r$ is the mean value of the difference between the velocity of two points located at distance r (Frisch (1995)).

If a high Reynolds number is assumed, so that a great separation of scales occurs, we may suppose that δ is large enough to be in the inertial range and the scales that appear in the integral are almost inertial. In this

way we may use the Kolmogorov relationship between $(\delta u)_r$ and r (that is $(\delta u)_r \sim \varepsilon^{1/3} r^{1/3}$, ε being the dissipation rate) for all the values of r smaller than δ, obtaining after integration the scaling law for angular momentum

$$h \sim \varepsilon^{\frac{1}{3}} \delta^{\frac{4}{3}} \tag{2.1}$$

This result is also obtainable using the Landau-Lifshits observation about the Loitsyanskij integral (see Yaglom & Monin (1975) or Landau & Lifshitz (1983)). They note that the angular momentum $\mathbf{H}$ of a volume V centered in the origin, in the limit of $V \to \infty$, is

$$\lim_{V \to \infty} \frac{\overline{\| \mathbf{H} \|^2}}{V} = 5\sqrt{2}\pi\rho^2\Lambda$$

where Λ is the Loitsyanskij integral

$$\Lambda = \int_0^{+\infty} r^4 B_{LL}(r) \mathrm{d}r \sim \int_0^{l_0} r^4 (\delta u)_r^2 \mathrm{d}r \sim \ell^5 E$$

where B_{LL} is the longitudinal correlation, ℓ the integral scale and E the turbulent kinetic energy. Then, for a volume of linear dimensions $\delta < l_0$ we can obtain the estimate

$$h \sim \frac{H}{\rho V_\delta} \sim \frac{\Lambda_\delta}{V_\delta} \sim \delta^{\frac{4}{3}} \varepsilon^{\frac{1}{3}},$$

which is identical to (2.1), and where we have used

$$\Lambda_\delta = \int_0^{\delta} r^4 u_r^2 \mathrm{d}r \sim \varepsilon^{\frac{2}{3}} \delta^{\frac{13}{3}}$$

The same scaling was shown by Yoshizawa (1982),Ferziger (1985) and Leaslie & Quarini (1979) to hold for the eddy viscosity. Effectively, Yoshizawa (1982) showed starting from a statistical analysis that, if a great divergence of scales is assumed, then the anisotropic part of the Reynolds "subgrid" tensor takes the form of an eddy viscosity multiplying the strain rate of the mean field, with ν_δ given by

$$\nu_\delta = c_\nu \, \delta^{\frac{4}{3}} \varepsilon^{\frac{1}{3}}, \quad c_\nu \approx 0.053 \tag{2.2}$$

This suggests a possible interesting usage of angular momentum in subgrid modelling: we may build a new differential model for the turbulent stresses based on a Boussineq transport hypothesis for the anisotropic part of the Reynolds subgrid stresses, in which the transport coefficient (the eddy

momentum budget	$\frac{\mathrm{D} < u_i >}{\mathrm{D}t}$	$\frac{\partial R_{ij}}{\partial x_j}$	pressure	viscous term
	1	ε^2	1	Re^{-1}
additional terms	0	ε^4	ε^2	$\varepsilon^2\mathrm{Re}^{-1}$
angular momentum budget	$\frac{\mathrm{D} < h_i >}{\mathrm{D}t}$	$\frac{\partial C_{ij}}{\partial x_j}$	pressure	viscous term
	1	1, ε^2	0	Re^{-1}
additional terms	0	ε^2, ε^4	0	$\varepsilon^2\mathrm{Re}^{-1}$

Table 2.1: Orders of magnitude of the different terms in the momentum and in the angular momentum balance equation after a proper adimensionalization, where $\varepsilon = \delta/L$ and L is the reference length. The additional terms are generated by the non-commutability of the spatial differentiation with the average operator when $\delta = \delta(\mathbf{x})$. Spherical averaging volumes are assumed.

viscosity) is taken proportional to the intrinsic angular momentum modulus of each average volume. That is, we write

$$\nu_\delta = ch, \quad h = (h_i h_i)^{\frac{1}{2}} \tag{2.3}$$

where c is the subgrid scale coefficient. Field $\mathbf{h}$ must be obtained from integration of equations (1.21), that nevertheless contain other nonlinear turbulent flow tensors that are to be represented with a model, namely (see §2.2 of chapter 1)

$$\begin{aligned} C_{ij} &= \varepsilon_{i\ell k}[(<x_l u_k> - <x_l><u_k>)\,<u_j> -(<x_l u_k u_j> - <x_l><u_k u_j>)] \\ M_{ij} &= \varepsilon_{i\ell k}[(<x_l T_{kj}> - <x_l><T_{kj}>] \end{aligned}$$

Tensor C_{ij} is of inertial origin and represents the angular momentum transport due to turbulent fluctuations while M_{ij} is the intrinsic angular momentum flow due to the molecular transport. If the average volume is spherical or in general the weighting function of (1.4) has spherical symmetry, the divergence of tensor $< M_{ij} >$ simply reduces to $\nu\nabla^2\mathbf{h}$, without adding any difficulty and which moreover may be also neglected at high Reynolds numbers. When averages without spherical symmetry are considered, it is composed by two parts, the pressure part whose principal part is of order δ^4 and the viscous part that scales as $\frac{1}{Re}\delta^2$. The other terms in the angular momentum balance (1.21) scale as δ^2.

From this it is easy to see that if δ is of the order of 10^{-2} the pressure part will be smaller than the viscous part for Reynolds numbers up to 10^4,

if δ is of the order of 10^{-3} the pressure part will be smaller than the viscous part for Reynolds numbers up to 10^{-6}, and so on. In table 1 the various order of magnitude of the terms in equations (1.19) and (1.21) are listed in the case of adoption of spherical volumes of integration. It is also shown the situation of the relative orders of magnitude when the spatial filter width δ is a function of the point, as it is necessary to adopt near to a wall where $\delta \to 0$ must be satisfied to apply the non slip boundary condition.

As a consequence in (1.21) the only term that needs to be modeled is C_{ij}. As customary, hypothesis are to be formulated on the transport phenomena that determine the angular momentum transport. The model we present is composed by two terms, the first of which is associated to the variation of scales and direction due to stretching and twisting phenomena, while the second term accounts for the angular momentum transport due to the fluctuations and has the structure of an auto diffusion:

$$C_{ij} = <u_i> h_j + c\, h\, (\partial_j h_i + \partial_i h_j - \frac{2}{3}\partial_s h_s \delta_{ij}) \tag{2.4}$$

where c is the same constant introduced in (2.3). As in the early works of Mattioli, we have assumed that the physical mechanisms of turbulent transport, due to small scale fluctuations, are almost the same for momentum and angular momentum transport. Moreover, we considered the effect of change of size of eddies to the stretching. This finally leads to transfer of energy between different scales, producing small scale fluctuations that increase turbulent transport. The hope is to include within this model this effect through the first term. This have also a counterpart in the series development of chapter one. In fact it is possible to obtain it as the δ^2 coefficient of the expansion of C_{ij}.

In regions of non homogeneous turbulence, where a gradient of integral scale is present, as in the numerical simulation we have carried out and that are described in the next chapter, will shall show how important may be the second order term of this development due to the high values the third order space derivatives of the velocity may reach.

A remark is needed about the mathematical structure that the insertion of the first term on the right hand side of (2.4) is attributing to equation (1.21) and in particular to the term consisting of the product of the filtered vorticity by the intrinsic angular momentum. Because of (2.11) this product may be, in the first approximation, represented by $h_j h_j$. If we set aside for a moment the non linear diffusive term, the structure of the equation could be considered analogous to the scalar non linear equation $\mathrm{d}_t s = s^2$, which develops a singularity in a finite time $s_0^{-1}, s_0 > 0$. We remind to the

extended analysis about the vorticity balance equation presented in Frisch (1995), pp. 115-117, for which no inviscid blow-up have been observed in numerical simulations of three dimensional Euler flows with smooth initial condition carried out by means of an *ad hoc* method able to single out eventual singularities.

From an operational point of view this model is close to the class of simple phenomenological theories of turbulent shear flows that introduce a rate equation for the turbulent viscosity, e.g. see Nee & Kovaznay (1969) or Germano (1991). It is still quite simple, since only one more equation - in this case vectorial - is added to the usual equation of motion. Moreover this equation contains only one constant to be determined from experiments, either made in laboratory or of numerical kind, as in Clark et al. (1979). In Nee & Kovasznay the approach was based on "educated-guess" concerning the physical function fulfilled by the various terms of the proposed transport scalar equation for the eddy viscosity. Our proposal is in the same way phenomelogical, in postulating a direct proportionality between eddy viscosity and angular momentum, where the rate equation added is now directly deduced from the conservation law of the moment of momentum.

A basic physical constraint for the turbulence description is its invariance with respect to changes of frame of reference. This requires, as noted by Speziale (1991), that the modeled Reynolds stress tensor, given its inertial nature, be form-invariant only under the extended Galilean group of transformations $\mathbf{x}^* = \mathbf{x} + c(t)\mathbf{n}$, which allows for arbitrary relative translation accelerations. This requirements is more severe than simple Galilean invariance but far less severe than that used in continuum mechanics, where form-invariance under arbitrary translations and rotations is considered. This model satisfy this invariance condition.

In conclusion, we propose a method of large, or perhaps better very large, eddy simulation based over the simultaneous integration of the volume averaged momentum and moment of momentum equations, that, even if our discussion is primary devoted to incompressible homogeneous flows, may be also useful for possible application to turbulent flows of suspension of generally shaped particles with inertia or with an external couple applied to them. In such situations the momentum equation might be coupled, through the antisymmetrical part of the bulk tensor, to an angular momentum equation.

1. 1 Evaluation of the model coefficient

Notwithstanding the introduction of an additional differential equation, only one subgrid constant c appears in the model. In this section this constant,

defined by equation (2.3), is estimated assuming that the largest resolvable wave number $2\pi/\delta$ lies within the inertial range, that the energy transfer rate from the resolved scales to the subgrid scales is equal to the energy dissipation rate ε and that a great separation of scales exists. In such a situation the energy of the subgrid scales is mostly that owned by their inertial part. Under this assumption Yoshizawa (1982) determined the constant of the scaling law for the eddy-viscosity, see equation (2.2).

The leading idea is to evaluate the constant in the scaling law (2.1). Considering average spherical volumes, of radius δ, we may write the intrinsic angular momentum h as

$$h \approx \frac{3}{4\pi\delta^3} \int_0^\delta (\delta u)_r 4\pi r^3 \mathrm{d}r, \tag{2.5}$$

where $(\delta u)_r$ is again the turbulent velocity variation over distances of the order r. The Kolmogorov's law yields

$$(\delta u)_r = (3\alpha)^{\frac{1}{2}} \left(\frac{\varepsilon r}{2\pi}\right)^{\frac{1}{3}},$$

where α is the Kolmogorov's constant, approximately equal to 1.5, value used by Lilly (1967). Integral (2.5) leads then to

$$h = c_h \varepsilon^{\frac{4}{3}} \delta^{\frac{1}{3}}, \quad c_h = \frac{9(3\alpha)^{\frac{1}{2}}}{13(2\pi)^{\frac{1}{3}}} \approx 0.80$$

When this equation is compared with (2.2), the constant c in (2.3) is consequently

$$c = \frac{c_\nu}{c_h} \approx 0.066.$$

This value has been successfully confirmed through a priori numerical test on homogeneous isotropic turbulence, see §4.1.

2. Wall boundary conditions and initial conditions

The use of this model requires the introduction of accessory conditions for **h**. As ever, difficulties concern the conditions at rigid non-slip boundaries. There are two possibilities: i) to keep the averaging linear scale constant and as a consequence to adopt approximated conditions at surfaces, parallel to the walls, but embedded into the flow, as done by Schumann (1975) for the momentum balance equation; ii) to let the linear scale δ to go to zero near the wall in order to apply there the exact condition $\mathbf{h} = 0$.

The first technique is based on the consideration that the LES method cannot be applied very close to the wall either in the viscous turbulent sublayer or in the transition region, because here the model of eddy viscosity fails since the local equilibrium has not yet reached. Shifting the frontiers inside the inertial zone, at a distance $\hat{y}$ from the wall, will allow the implementation of the same turbulence model uniformly in all the domain. This is accomplished by placing the first grid point at a distance Δ from the wall equal to $2 \sim 3\%$ of the entire thickness of the boundary layer. If the flow satisfy the conditions of parallelism and stationarity in the mean the time averaged velocity $\overline{u}_1$ and the tangential stress $\overline{\tau}_{\hat{y}}$ will satisfy, according to Schumann (1975), the relation

$$< u_1(\mathbf{x}, t) >= \frac{\overline{u}_1}{\overline{\tau}_{\hat{y}}} \nu_\delta \frac{\partial < u_1 >}{\partial y} \tag{2.6}$$

where $\overline{\tau}_{\hat{y}}$ is the time averaged wall tangential stress assumed constant across the inner layer ($\sim$ first 5 %) and $\overline{u}_1$ is the time mean value of the longitudinal velocity component described by the logarithmic law of the wall.
By analogy we may extend this assumption to the treatment of the intrinsic angular momentum boundary conditions. That would mean to put, for $\mathbf{h}$ defined as in (1.20):

$$\mathbf{h} = \frac{\|\overline{\mathbf{h}}\|}{\|<\boldsymbol{\omega}>\|} <\boldsymbol{\omega}> \quad y = \Delta \approx 2\delta. \tag{2.7}$$

On the other hand if one estimates the time mean value of $\mathbf{h}$ by using the wall law one would easily verify that

$$\overline{h} = \frac{1}{4k} \Delta u_* = (\frac{\Delta^2}{4}) \frac{\partial \overline{u}_1}{\partial y}|_{y=\Delta} = (\frac{\Delta^2}{4}) \frac{\partial < u_1 >}{\partial y}|_{y=\Delta},$$

where k is the Von Karman constant, u_* is the wall velocity. An improvement to the Schumann's assumption, according to the experimental findings by Rajagopalan and Antonia (1979), was proposed by Piomelli, Ferziger & Moin (1989) through the introduction of a time delay between the velocity in the logarithmic region and the wall stress. However, this type of conditions may be implemented only in presence of a direction of homogeneity, as in the channel or in the pipe flows.

Where this is not the case, the situation gets much more complicated. The region close to the wall must be described, as a consequence one must allow the integration grid to go to zero at the wall to apply the correct non slip boundary condition $\mathbf{h} = \mathbf{0}$. Two are the problems to face with.

The first is that the grid points must be necessarily addensed close to the wall in regions that supposedly simulate the viscous and transition sublayers, where the general turbulence model is no more valid. Beginning eighties the researchers carrying out numerical computation were used to introduce wall functions attenuating the weight of the eddy viscosity, with respect to the molecular viscosity, into the adopted model, see for example Piomelli, Ferziger & Moin (1989) and Moin & Kim (1982). More recently, 1992 and beyond, an alternative tool to the wall function use came from the dynamic subfilter model by Germano (1992) that allows the local determination of the mixing length in the Smagorinsky eddy viscosity model.

The second problem is related to the loss of the commutability property between the spatial filtering and the differentiation operations and was already considered in section 2.4 of chapter 1, where an approximation based on two different level of nested averages was proposed.

As for the initial conditions, the model here proposed has no special requirements with respect to the standards: the initial velocity field, and thus the initial angular momentum field, are generated possibly on a finer grid than the one afterward used for the simulation, through algorithms producing a spatial distribution of random numbers satisfying the solenoidal property and the prescribed energy spectrum.

3. Numerical procedure for the validation of the model

When dealing with a new model, a validation is needed in order to asses its capability of reproducing the key features of real flows. This is customary done solving the equations in simple situations for which a great amount of experimental or theoretical information is available. Turbulent flows with these characteristics are, for example, homogenous isotropic turbulence, homogeneous shear flows and turbulent boundary layers.

The special case of a large eddy model admits an other type of test, based on the availability of data coming from direct numerical simulation. This test, first suggested by Clark et al. (1979), consists in the direct computation of quantities that need to be described by a model through direct average of the velocity field and their comparison with model prevision for the same flow. This test does not need to perform any simulation and is called *a priori* test. Although limited to the low Reynolds numbers of present direct numerical simulations, it may be considered a more fundamental test because of the integrated nature of the results of large-eddy simulations, which combine the model adopted with the effects of spatial and temporal discretization and of averaging.

The second test we performed was a simulation of the simplest turbulent flow, homogeneous isotropic decaying turbulence. This is a flow which has been widely studied, and which, for its particular configuration, simplifies the numerics to be used because avoids the problems due to the presence of rigid wall boundaries.

Results of these tests are presented in the following section. Here a brief survey of the numerical procedures used to perform them is given. A code based on spectral methods for spatial discretization in conjunction with explicit low storage Runge-Kutta method for temporal integration was developed to fit in with the model validation. The details about the implementation may be found in Iovieno & Tordella (2001).

3. 1 Spatial discretization

We have to solve the following equations

$$\nabla \cdot \mathbf{u} = 0 \tag{2.8}$$

$$\partial_t \mathbf{u} = \mathbf{A}(\mathbf{u},\mathbf{h}) \equiv -\nabla p + \nabla \cdot (-\mathbf{u}\otimes\mathbf{u} + (\nu + ch)(\nabla\mathbf{u} + \nabla^T\mathbf{u})) \tag{2.9}$$

$$\partial_t \mathbf{h} = \mathbf{B}(\mathbf{u},\mathbf{h}) \equiv \nabla \cdot (\mathbf{u}\otimes\mathbf{h} - \mathbf{h}\otimes\mathbf{u} + (\nu + ch)(\nabla\mathbf{h} + \nabla^T\mathbf{h}) - \frac{2}{3}\nabla\cdot\mathbf{h}\,\mathbf{I}) \tag{2.10}$$

where $h = \| \mathbf{h} \|$, on the cube $(0, 2\pi)^3$ with periodic boundary conditions

$$\mathbf{u}(\mathbf{x} + 2\pi\mathbf{e}_i, t) = \mathbf{u}(\mathbf{x}, t) \quad i = 1, 2, 3 \tag{2.11}$$

$$\mathbf{h}(\mathbf{x} + 2\pi\mathbf{e}_i, t) = \mathbf{h}(\mathbf{x}, t) \quad i = 1, 2, 3 \tag{2.12}$$

In this section we partially depart from our convention of denoting with brackets spacial averaged variables to avoid unnecessary complicated notations, and so we shall write $\mathbf{u}$ instead of $<\mathbf{u}>$. Likewise, the vector notation will be often preferred to limit the proliferation of indexes. Problem (2.8-2.12) is well suited for the use of a spectral spatial discretization due to the very simple geometry of the flow domain, and in particular for a Fourier-Galerkin method. Spectral methods belong to the class of discretization schemes known generically as the method of the weighted residuals, of which they may be viewed as a special subset. Two are the key elements of this class of methods: the trial functions, also called the expansion or approximating functions, and the test functions, also known as weight functions. The trial functions are used as the basis functions for a truncated series

expansion of the solution while the test functions are used to ensure that the original differential equation to solve is satisfied as closely as possible by the truncated series expansion. This is achieved by requiring that the residual satisfies a suitable orthogonality condition with respect to all the test functions.

The choice of the trial functions is one of the features that distinguish spectral methods from other discretization schemes like finite difference and finite element methods. The trial functions for spectral methods are indefinitely differentiable global functions. In the case of finite elements methods, the domain is divided into smaller elements on which a smooth trial function is defined. The trial functions are then local in character, and well suited for handling complex geometries, but they are not indefinitely differentiable in the whole domain. Finite difference trial functions are likewise local. This explains the difference in convergence rates for spectral methods as contrasted to other methods, that is the convergence rate for spectral methods depends only on the smoothness of the solution. The choice of test functions distinguishes between the different spectral schemes, namely the Galerkin, collocation and tau schemes. Spectral methods are distinguished also by the particular choice of the trial functions. Details are in Canuto et al. (1988).

In the Galerkin approach, that will be used in the following, the test functions are the same as the trial functions. They are, therefore, infinitely smooth functions which individually satisfy the boundary conditions. The differential equation is enforced by requiring that the integral of the residual by each test function to be zero. This is equivalent to require that the residual keeps a minimum in the vector space of test and trial functions.

A spectral Galerkin method is practical for high-resolution calculations of non linear problems only when transform methods for evaluating convolution sums arising from quadratic non-linearities are available. Non-linear term more complicated then quadratic non-linearities make spectral Galerkin unpractical. Problem (2.8-2.10) and all fluid dynamics problems in general contain only such non-linearities and then enable the use of these methods.

We look for a solution which is periodic in the hyper-interval $(0, 2\pi)^3$, so that the natural and convenient choice is to take both the trial functions space and the test function space as the set of all trigonometric polynomials of degree $\leq N/2$. The approximate solution $(\mathbf{u}^N, \mathbf{h}^N)$ is then represented in the form of a truncate Fourier series

$$\mathbf{u}^N(\mathbf{x},t) = \sum_{k=-\frac{N}{2}}^{\frac{N}{2}-1} \hat{\mathbf{u}}_{\mathbf{k}}^N(t)\mathrm{e}^{i\mathbf{k}\cdot\mathbf{x}} \tag{2.13}$$

$$\mathbf{h}^N(\mathbf{x},t) = \sum_{k=-\frac{N}{2}}^{\frac{N}{2}-1} \hat{\mathbf{h}}_{\mathbf{k}}^N(t)\mathrm{e}^{i\mathbf{k}\cdot\mathbf{x}} \tag{2.14}$$

where $\mathbf{k}$ is the three dimensional wavenumber $\mathbf{k} = (k_1, k_1, k_3)$.

The expansion in terms of an orthogonal system introduces a linear transformation between functions $\mathbf{u}$, $\mathbf{h}$ and the sequence of their coefficients $\hat{\mathbf{u}}_{\mathbf{k}}^N$ and $\hat{\mathbf{h}}_{\mathbf{k}}^N$ to which the unknowns of the problem are shifted. For their computation special numerical procedures were developed, in particular the most efficient is the Fast Fourier Transform (FFT) (Brigham (1974)) that allows the computation of the discrete one-dimensional transform at the cost of only $\sim \frac{5}{2}N\log_2 N$ instead of $O(N^3)$ operations of a direct use of its definition when the simplification of having real functions is taken in account. The three dimensional transform can be computed by means of successive iterations of the one dimensional transform; this requires N^2 transforms for a total of about $\frac{15}{2}N^3\log_2 N$ operations. Equations for $\hat{\mathbf{u}}_{\mathbf{k}}^N$ and $\hat{\mathbf{h}}_{\mathbf{k}}^N$ are obtained by requiring the residual of (2.8-2.10) to be orthogonal to all the test functions. With the inner product of L^2 this leads to

$$\int_0^{2\pi} (\nabla\cdot\mathbf{u}^N)\mathrm{e}^{-i\mathbf{k}\cdot\mathbf{x}}\mathrm{d}\mathbf{x} = 0 \tag{2.15}$$

$$\int_0^{2\pi} (\partial_t\mathbf{u}^N - \mathbf{A}(\mathbf{u}^N,\mathbf{h}^N))\mathrm{e}^{-i\mathbf{k}\cdot\mathbf{x}}\mathrm{d}\mathbf{x} = 0 \tag{2.16}$$

$$\int_0^{2\pi} (\partial_t\mathbf{h}^N - \mathbf{B}(\mathbf{u}^N,\mathbf{h}^N))\mathrm{e}^{-i\mathbf{k}\cdot\mathbf{x}}\mathrm{d}\mathbf{x} = 0 \tag{2.17}$$

Using expressions (2.13) and (2.14) and performing the analytical spatial differentiation of the trial functions, due to the orthogonality property of trigonometric polynomials, we obtain

$$i\mathbf{k}\cdot\mathbf{u}^N = 0 \tag{2.18}$$

$$\partial_t\hat{u}_{i,\mathbf{k}}^N = \hat{A}_{i,\mathbf{k}} \equiv -ik_j\widehat{(u_j u_i)}_{\mathbf{k}} - ik_i\hat{p}_{\mathbf{k}}^N - \nu k^2\hat{u}_{i,\mathbf{k}}^N + \\ +ik_j\widehat{(h(\partial_j u_i + \partial_i u_j))}_{\mathbf{k}} \tag{2.19}$$

$$\begin{aligned}\partial_t \hat{h}^N_{i,\mathbf{k}} &= \hat{B}_{i,\mathbf{k}} \equiv -ik_j(\widehat{(u_j h_i)}_{\mathbf{k}} - (\widehat{h_j u_i})_{\mathbf{k}}) - \nu k^2 \hat{h}^N_{i,\mathbf{k}} + \\ &+(h(\partial_j h_i + \widehat{\partial_i h_j} - \frac{2}{3}\partial_s h_s)_{\mathbf{k}} \end{aligned} \tag{2.20}$$

Pressure may be eliminated performing the scalar product of $\mathbf{k}$ times (2.19) and using (2.18). This is the Fourier correspondent of the projection onto the divergence-free vector functions.

If it were merely an approximation problem, then $\mathbf{u}^N_{\mathbf{k}}$, $\mathbf{h}^N_{\mathbf{k}}$ would be the truncated Fourier series of known functions; for a partial differential equation, however, the approximation (2.13-2.14) is determined by (2.18-2.20), of which they are the solution. The k-th coefficient of the expansion decays faster then any inverse power of k (that is, exponentially) when the function is infinitely smooth (Rudin (1974)). In practice this decay is not exhibited until there are enough coefficients to represent all the essential structures of the function. The subsequent rapid decay of the coefficients implies that the Fourier series truncated after just a few more terms represents an exceedingly good approximation of the function. This characteristic is usually referred to as "spectral accuracy" of the Fourier method and implies an exponential error decay for large N.

As it is evident from (2.18-2.20), a principal algorithmic component of an efficient Fourier-Galerkin method for a nonlinear problem as that we are going to solve is the evaluation of convolution sums that arise from quadratic nonlinearities in (2.18-2.20) and from the computation of h. In particular, being the transform coefficient our unknowns, we must define a procedure to obtain the discrete Fourier coefficients of a product from the Fourier coefficients of the factors. Let us focus on the treatment of a general quadratic term

$$w(\mathbf{x}) = u(\mathbf{x})v(\mathbf{x})$$

In the case of an infinite Fourier series expansion, we have the well known convolution sum (Rudin (1974))

$$\hat{w}_{\mathbf{k}} = \sum_{\mathbf{m}+\mathbf{n}=\mathbf{k}} \hat{u}_{\mathbf{m}}\hat{v}_{\mathbf{n}}, \qquad \hat{w}_{\mathbf{k}} = \frac{1}{2\pi}\int_0^{2\pi} w(\mathbf{x})e^{-i\mathbf{k}\cdot\mathbf{x}}\mathrm{d}\mathbf{x}$$

Instead when u, v, w are approximated by their respective truncated Fourier series of degree $N/2$, the convolution sum becomes

$$\hat{w}_{\mathbf{k}} = \sum_{\mathbf{m}+\mathbf{n}=\mathbf{k},|\mathbf{m}+\mathbf{n}|<N/2} \hat{u}_{\mathbf{m}}\hat{v}_{\mathbf{n}}$$

where $k \leq N/2$. The direct summation implied by the discrete convolution sum takes roughly $O(N^4)$ operations in three dimension, that makes this prohibitively expensive from a computational point of view. The use of transformation methods, as first proposed by Rogallo, enables this to be computed with only $O(N^3 \log_2 N)$ operations, that is at the cost of two discrete tranform with FFT algorithm: The approach taken in the transform method is to use the inverse discrete transform to transform $\{\hat{u}_{\mathbf{m}}\}$ and $\{\hat{v}_{\mathbf{n}}\}$ to physical space, to perform there the pointwise multiplication in the grid points and then to use the discrete transformation to determine $\hat{w}_{\mathbf{k}}$. In this way we have

$$\hat{w}_{\mathbf{k}} = \frac{1}{N} \sum_{j=0}^{N-1} w(x_j) e^{-i\mathbf{k}\cdot\mathbf{x_j}} = \frac{1}{N} \sum_{j=0}^{N-1} u(\mathbf{x_j}) v(\mathbf{x_j}) e^{-i\mathbf{k}\cdot\mathbf{x_j}} \tag{2.21}$$

after inserting the discrete expansion of u and v,

$$u(\mathbf{x}, t) = \sum_{|\mathbf{k}| \leq \frac{N}{2}} \hat{u}_{\mathbf{k}} \mathrm{e}^{i\mathbf{k}\cdot\mathbf{x}}$$

$$v(\mathbf{x}, t) = \sum_{|\mathbf{k}| \leq \frac{N}{2}} \hat{v}_{\mathbf{k}} \mathrm{e}^{i\mathbf{k}\cdot\mathbf{x}}.$$

With the use of the orthogonality relation between trigonometric polynomials, this leads us to

$$\begin{aligned}
\hat{w}_{\mathbf{k}} = & \sum_{\mathbf{m}+\mathbf{n}=\mathbf{k}} \hat{u}_{\mathbf{m}}\hat{v}_{\mathbf{n}} + \\
& + \sum_{\mathbf{m}+\mathbf{n}=\mathbf{k}\pm N\mathbf{e}_1} \hat{u}_{\mathbf{m}}\hat{v}_{\mathbf{n}} + \sum_{\mathbf{m}+\mathbf{n}=\mathbf{k}\pm N\mathbf{e}_2} \hat{u}_{\mathbf{m}}\hat{v}_{\mathbf{n}} + \sum_{\mathbf{m}+\mathbf{n}=\mathbf{k}\pm N\mathbf{e}_3} \hat{u}_{\mathbf{m}}\hat{v}_{\mathbf{n}} + \\
& + \sum_{\mathbf{m}+\mathbf{n}=\mathbf{k}\pm N\mathbf{e}_1\pm N\mathbf{e}_2} \hat{u}_{\mathbf{m}}\hat{v}_{\mathbf{n}} + \sum_{\mathbf{m}+\mathbf{n}=\mathbf{k}\pm N\mathbf{e}_1\pm N\mathbf{e}_3} \hat{u}_{\mathbf{m}}\hat{v}_{\mathbf{n}} + \sum_{\mathbf{m}+\mathbf{n}=\mathbf{k}\pm N\mathbf{e}_2\pm N\mathbf{e}_3} \hat{u}_{\mathbf{m}}\hat{v}_{\mathbf{n}} + \\
& + \sum_{\mathbf{m}+\mathbf{n}=\mathbf{k}\pm N\mathbf{e}_1\pm N\mathbf{e}_2\pm N\mathbf{e}_3} \hat{u}_{\mathbf{m}}\hat{v}_{\mathbf{n}}
\end{aligned} \tag{2.22}$$

The first term is the correct value of $\hat{w}_{\mathbf{k}}$, the next three terms are the singly-aliased contributions, the next three are the doubly-aliased contributions and the last term is the triply-aliased contribution to the convolution. Several techniques were developed to avoid aliasing errors, see Canuto et al. (1988) for a review. We use the truncation or padding technique. The key to this dealiasing technique is the use of a discrete transform with $M > N$ rather then N points in each direction, in order to have more Fourier coefficients and then to correctly compute the first N coefficients of (2.21).

Let us expand $\{\hat{u}_{\mathbf{m}}\}$ and $\{\hat{v}_{\mathbf{n}}\}$ as

$$\tilde{u}_{\mathbf{k}} = \begin{cases} \hat{u}_{\mathbf{k}} & \max_i \mid k_i \mid \leq \frac{N}{2} \\ 0 & \text{otherwise} \end{cases} \qquad \tilde{v}_{\mathbf{k}} = \begin{cases} \hat{v}_{\mathbf{k}} & \max_i \mid k_i \mid \leq \frac{N}{2} \\ 0 & \text{otherwise} \end{cases} \tag{2.23}$$

Thus, coefficients of $\{\tilde{u}_{\mathbf{m}}\}$ and $\{\tilde{v}_{\mathbf{n}}\}$ are the $\{\hat{u}_{\mathbf{m}}\}$ and $\{\hat{v}_{\mathbf{n}}\}$ "padded" with zeros in the additional wavenumbers. Using the inverse discrete transform operating with M points, calculating the product in the physical space and then transforming again with M points, one gets the equivalent of (2.22), with N substituted by M. We are clearly interested only in $\tilde{w}_{\mathbf{k}}$ for $\mid k_i \mid \leqslant N/2$, and now the advantage of performing the product with more points is evident: we may choose M such that the aliasing terms in the right hand side of the equivalent of (2.22) vanish for each $\mathbf{k}$ such that $\mid k_i \mid \leq N/2$. Since $\tilde{u}_{\mathbf{m}}$ and $\tilde{v}_{\mathbf{n}}$ are zero for $\mid m_i \mid > N/2$, $\mid n_i \mid > N/2$, this condition requires that

$$-\frac{N}{2} - \frac{N}{2} \leq \frac{N}{2} - 1 - M$$

that is $M \geq \frac{3N}{2} - 1$. So, we choose $M = 3N/2$, the minimum value that assures the aliasing error removal. With this statement, we obtain an aliasing free convolution sum at the cost of two transforms with a greater amount of points. The total amount of operations is $\frac{45}{4} N^3 \log_3 \frac{3}{2} N$, which is only about one half greater then the aliased method. For obvious reasons this technique is sometimes referred to as the $\frac{3}{2}$-rule. When compared with other methods developed for complete de-aliasing, like phase-shift, this technique is the most convenient considering the amount of operations (Canuto et al. (1988)). Furthermore, it is easy to implement, a not negligible advantage in practical computations. The only numerical disvantage is that the routine that performs the computation of products has to handle vectors with total dimension up to $M^3 = \frac{9}{4} N^3$, that is about two times larger, requiring consequently a bit more memory. The details of the implementation are described in Iovieno & Tordella (2001).

3. 2 Time discretization

The semi-discretized ordinary differential equations (2.18-2.20) require the adoption of a time-discretization scheme in order to be solved numerically. They fit in with the general form

$$\partial_t v = F(v)$$

of an autonomous system, if we write $v = (\hat{\mathbf{u}}_\mathbf{k}, \hat{\mathbf{h}}_\mathbf{k})$ and $F = (\hat{A}_\mathbf{k}, \hat{B}_\mathbf{k})$. Inasmuch as they are ordinary differential equations, a wide set of methods are available. The spatial discretization adopted is a spectral one, and then of infinite order, so it is useful to adopt high order schemes. Three requirements are to be considered when choosing the temporal discretization scheme and the time step: accuracy, stability and computation time. When dealing with spectral methods, stability is a far more severe constrain than accuracy. Even if implicit methods have in general a larger asymptotic stability region than the explicit one, they require the solution of an additional equation at each time step, to be solved with iterative schemes and which needs special ad hoc methods because the matrices coming from the spectral spatial discretization are not sparse (Canuto et al. (1988)). To avoid too many code complexity, we decided to use explicit methods, and two classes of methods were evaluated: the standard one step Runge-Kutta schemes (RK) and the multistep Adam-Bashford-Backward Differentiation Euler schemes. The latter may be viewed as a modification of the classical Adam-Bashford schemes with a larger stability region. In particular, we used a 4-th order Runge-Kutta in the low storage version by Jameson, Schmidt and Turkel (1981) for autonomous systems,

$$\begin{aligned} v_1 &= v^n + \frac{1}{4}F(v^n) \\ v_2 &= v^n + \frac{1}{3}F(v_1) \\ v_3 &= v^n + \frac{1}{2}F(v_2) \\ v^{n+1} &= v^n + F(v_3) \end{aligned}$$

that requires four evaluations of function F for each step like all 4-th order Runge-Kutta schemes, but that requires the storage of only one additional vector other than v^n and v^{n+1} for each step as contrasted to the four additional vectors storage required by standard RK4, as we can see by its implementation

$$\begin{aligned} v &\leftarrow v^n + \frac{1}{4}F(v^n) \\ v &\leftarrow v^n + \frac{1}{3}F(v) \\ v &\leftarrow v^n + \frac{1}{2}F(v) \\ v^{n+1} &\leftarrow v^n + F(v) \end{aligned}$$

and the third order AB/BDE (Peyret (1999)),

$$v^{n+1} = \frac{6}{11}[3v^n - \frac{3}{2}v^{n-1} + \frac{1}{3}v^{n-2} + \Delta t(3F(v^n) - 3F(v^{n-1}) + F(v^{n-2}))]$$

that requires only one evaluation of function F for each step, but uses information from the three preceeding time steps, needing then two additional levels of storage. A multistep method requires a special implementation in the first few time steps, where a one step scheme is necessary. The choice of the single step scheme needs careful considerations because the error introduced will be propagated through the entire simulation. Our first idea was to couple AB-BDE3 with RK4 for the initial two steps, but considerations of convenience led us to the use of RK4 for the entire simulation. In fact, the region of asymptotic stability of a one-step method increases with the order of the method, while the region of asymptotic stability of a multistep method decreases as the order of the method increases. As an effect, the region of stability of AB/BDE3 is about three times smaller then the region of RK4, particularly near the imaginary axis, requiring consequently a time step three times smaller. This reduces the advantage of a multistep method in terms of saving of computation time due to fewer function F evaluations. In all simulations even performed was used RK4 alone.

Standard general results for stability are only known for linear systems. In all the other cases suggestions to linearize equations and to compute eigenvalues of the linearized system to estimate the stability constrain on the time step are given. However, inertial terms that have an important role in the dynamics of the large scales of turbulence are missed in a linearization about a mean value of velocity equal to zero in homogeneous turbulence. So, the linearized form reduces to a diffusive equation with preserves too little information about the whole system. We decided instead to consider as reference model the linear problem with

$$\begin{aligned} \hat{\mathbf{A}}_\mathbf{k} &\sim iak\mathbf{u}_\mathbf{k} - bk^2\mathbf{u}_\mathbf{k}, \\ \hat{\mathbf{B}}_\mathbf{k} &\sim iak\mathbf{h}_\mathbf{k} - idk\mathbf{u}_\mathbf{k} - bk^2\mathbf{h}_\mathbf{k}. \end{aligned}$$

Coefficients a, b, d were chosen as

$$a = 2E^{\frac{1}{2}}, \quad b = \nu + ch, \quad d = h$$

where here E is the turbulent kinetic energy, and h the modulus of angular momentum averaged in the whole domain. Eigenvalues of this problem

are clearly $\lambda \sim iak_j - bk^2$ and may be used to estimate the maximum allowable value of the time step using the standard diagrams for the region of asymptotic stability (Peyret (1999)). The maximum allowable time step was found to be about 0.07 simulation units for 32^3 computations. This estimate proved to be conservative.

3. 3 Initial conditions

Initial conditions are obtained from the NASA-Agard datasheet by Wray (1998). It contains one instantaneous velocity field at $\mathrm{Re}_\lambda = 104.5$ of a 512^3 direct numerical simulation of homogeneous isotropic decaying turbulence performed by Wray together with time evolutions of some statistics, like energy, energy spectra, enstrophy and dissipation. From these data we computed the space averaged Les fields through spatial average in cubic volumes. Although the DNS data are in the physical space, it is more to convenient operate in the wavenumber transform space where convolution integrals are substituted by multiplications and subsequent truncation of the Fourier coefficients. Let us call with a tilde the coefficient of the discrete transform with the DNS N_W points. We have for the velocity

$$\hat{\mathbf{u}}_\mathbf{k} = \tilde{\mathbf{u}}_\mathbf{k}\tilde{g}_\mathbf{k}, \quad \tilde{g}_\mathbf{k} = \prod_{j=1}^{3} \frac{\sin k_j\delta}{k_j\delta} \quad \forall \mathbf{k}, \mid k_j \mid \leq \frac{N}{2}$$

The angular momentum was defined in chapter 1 as

$$h_i = \varepsilon_{i\ell m}\frac{1}{V_\delta}\int_{\mathcal{I}_\delta} \eta_\ell u_m(\mathbf{x}+\boldsymbol{\eta})\mathrm{d}\boldsymbol{\eta}$$

Substituting the expansion of the velocity field we have, for the Fourier coefficients of $\mathbf{h}$, the following expression

$$(\hat{h}_i)_\mathbf{k} = \varepsilon_{i\ell m}\frac{(\hat{u}_m)_\mathbf{k}}{k_\ell}\left(\cos(k_\ell\delta) - \frac{\sin(k_\ell\delta)}{k_\ell\delta}\right)\prod_{j\neq\ell}\frac{\sin k_j\delta}{k_j\delta}$$

The choice of the linear dimension δ is based on the uniform grid spacing, $\delta = 2\pi/N$ in simulation units.

4. Model validation

4. 1 A priori test

The *a priori* test is based on the availability of a direct numerical simulation full turbulent velocity field. This availability allows to compute all variables

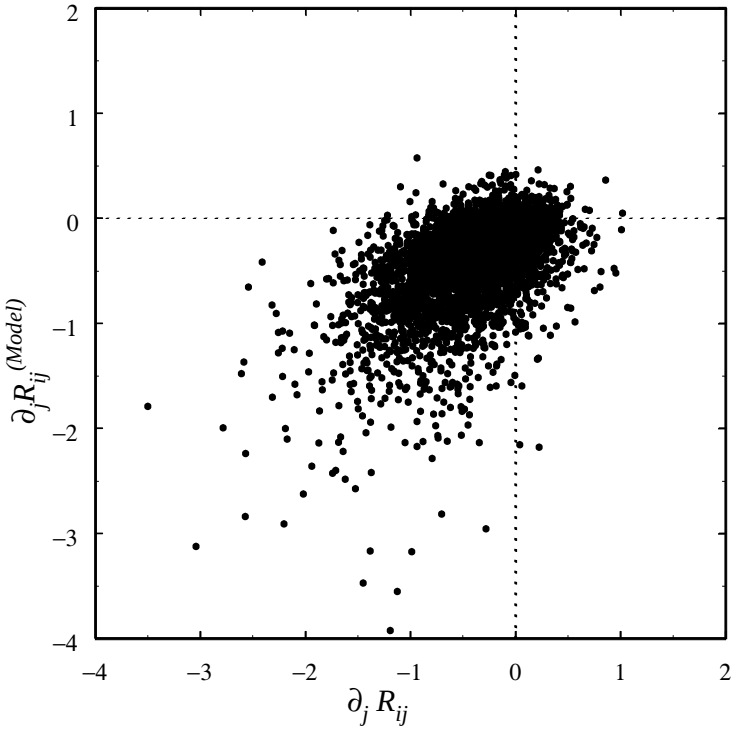

Figure 2.1: Scatter plot of comparison between experimental values and model predictions at vector level. Correlation level is about 0.45.

that are described by the model.

These data, as first suggested by Clark et al. (1979), are used to compute the small scale dependent quantities that require a model in the averaged motion equation. They are compared with the model prediction obtained for the same flow realization from the averaged variables.

According to Clark et al. (1979), we used the correlation between the model prediction and the directly computed quantities for the comparison. This correlation is defined as usual as the normalized covariance

$$C(X,M) = \frac{\overline{\left(X-\overline{X}\right)\left(M-\overline{M}\right)}}{V(X)^{\frac{1}{2}}V(M)^{\frac{1}{2}}}, \tag{2.24}$$

where X is the exact 'experimental' value and M the prediction of the model, $V(X)$ and $V(M)$ are their variance and the bar denotes the average over the entire computational domain. Several variables may be considered, depending on their physical significativity. We considered three levels of comparison: a tensorial level, between the volume averaged Reynolds stresses, a vectorial level, between the divergences of the Reynolds stresses (the most relevant quantity since it is the one that actually occurs in the momentum equation) and lastly a scalar level, between the scalar product of the divergence of the Reynolds stresses and the velocity, that relates to the capability of the model to describe a correct energy dynamics. That is, quantity X in (2.24) was in turn

$$X = R_{ij}, \;\; \partial_j R_{ij}, \;\; <u_i> \partial_j R_{ij}$$

where R_{ij} are the turbulent Reynolds "subgrid" stresses defined in chapter 2. All quantities were computed through spatial average on cubic volumes of the DNS velocity field by Wray. Integration was carried out analytically by integrating the Fourier polynomials that interpolate the data on the finer DNS grid in the same way as discussed in previous section for the computation of the initial conditions. The dealiased padding procedure for the evaluation of the products was also implementated.

We obtained correlations of about 0.40 at tensorial level, 0.45 at vectorial level and 0.92 at scalar level. A scatter plot of this comparison is shown in figure 2.1. These are encouraging values, better than those illustrated by Clark et al. (1979) or McMillan & Ferziger (1979) for other classical eddy viscosity models (the improvement is of about 30%) - i.e. Smagorinsky's, vorticity, turbulent kinetic energy and constant eddy viscosity - which, however, were all been obtained working on a different database. However, when we repeated this test for the above models as applied to Wray's bata sheet, we observed that their correlation values were rising and were approaching those of the present model. As a consequence no real superiority of this model may be claimed: slight differences in data bases, apparently statistically similar, may have strong influences on the results. This confirms the conclusion drawn in Clark et al. (1979) that all the models based on the molecular diffusion analogy - eddy viscosity type models - are roughly equally valid.

From these data it is also possible to estimate the value of the coefficient of the model by means of the least square procedure. Values founded are of about 0.066 ± 0.005 for all data processed. This estimate is in good agreement with the theoretical evaluation of section 1.1.

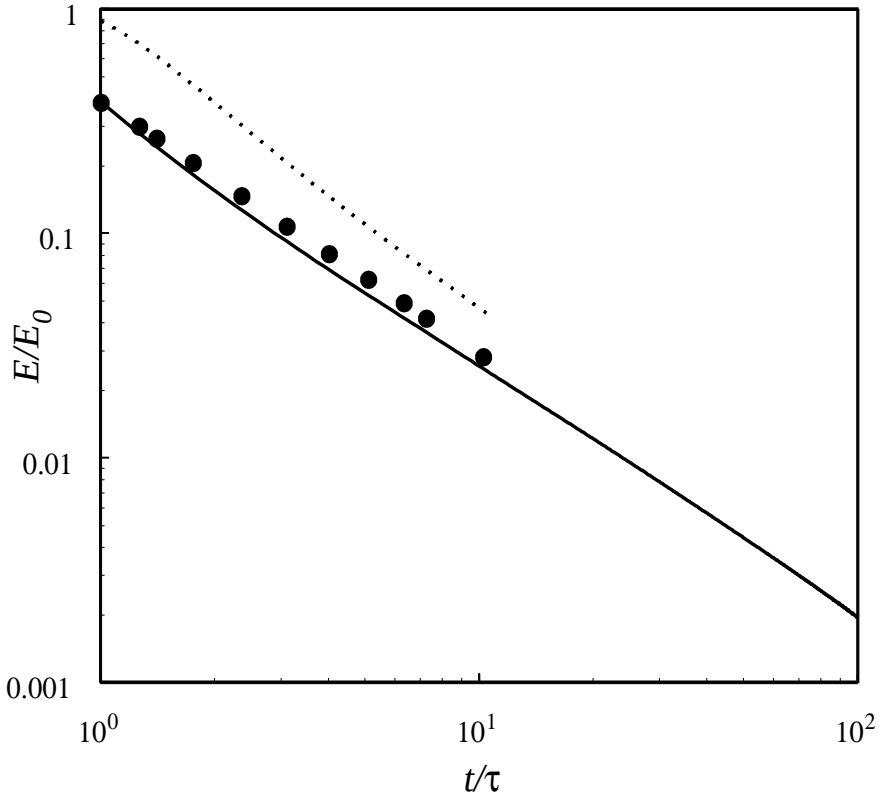

Figure 2.2: Decay of homogeneous isotropic turbulence. Dotted line refers to Wray's DNS, continous line is our 32^3 simulation and dots are the energy of the filtered field reconstructed from Wray's three dimensional spectra.

4. 2 Homogeneous isotropic decaying turbulence

The simplest possible flow field, homogeneous isotropic turbulence, for which a wide body of results is available, either theoretical either coming from numerical or laboratory experiments, was chosen as first test of the performances of the angular momentum model applied to incompressible flows. The experimental grid turbulence is simulated by solving the averaged equations within a cubic domain with periodical boundary conditions on his faces, see §3.1. A discussion of the numerical procedure used was already given in previous section.

The first physical quantity we checked was the decay of kinetic energy. Using the same coefficient obtained with least squares procedure applied on

the *a priori* test, we found that the decay matches with a power law with an exponent of about -1.23, in good agreement with grid turbulence experiments (Comte-Bellot & Corrsin (1971)) and with the recent theoretical analysis of Speziale (1992). We pursued the computation of the decay until 100 time units, but we could neither see any significative approach of the exponent to unity as predicted by the analysis by Speziale (1992) as asymptotic limit nor a variation announcing the theoretical asymptotic value of -2.5 for the final stage of decay dominated by viscosity, see Batchelor (1953). A further marching on time was impossible since the flow macroscale was becoming too big with respect to the domain dimension. The high correlation obtained at the scalar level explains the successful prediction of energy decay in the simulation object of the second validation test we performed. As customary in homogeneous turbulence, statistical averages are replaced by spatial averages on the entire volume. Figure 2.2 shows the decay we obtained and the one found by Wray in his simulation. The levels of energy are different because our initial field of volume averaged velocities possesses only a fraction of the total kinetic energy of the DNS field. A complete comparison needs clearly to filter the DNS velocity field in order to have data with the same physical content. This would be easy to perform if the data of the full simulation were available. Unfortunately, this is not the case. However, we could recover this through the three dimensional energy spectrum that is reported in a few instants in the *AGARD* database. Dots in figure 2.2 are obtained integrating the three dimensional energy spectra in the range of wavenumbers of our simulation,

$$E_f = \int_0^{k_f} E_{3D}(k)\mathrm{d}k$$

where k_f is the maximum wavenumber of our 32^3-simulation.

A more severe test than global energy decay are correlations and energy spectra. In homogeneous isotropic turbulence the one-time correlation tensor

$$\mathcal{R}_{ij}(\mathbf{r},t) = \overline{u_i(\mathbf{x},t)u_j(\mathbf{x}+\mathbf{r},t)} \tag{2.25}$$

is by definition isotropic and reduces for decaying turbulence to $\mathcal{R}_{ij}(\mathbf{r},t) = 2E(t)f(r)\delta_{ij}$, where $E(t) = \frac{1}{2}\overline{u_i(\mathbf{x},t)u_i(\mathbf{x},t)}$ (Batchelor (1953)). We checked both the isotropy computing the diagonal components $R_{11}(r\mathbf{e_1},t)$, $R_{22}(r\mathbf{e_2},t)$, $R_{33}(r\mathbf{e_3},t)$ of the correlation tensor and the self-similarity of decay. Deviation from isotropy is less then 8%. Similar results are also obtained for the energy spectra plotted in figure 2.3.

The scaling law (2.1) for angular momentum may be expressed as $h \sim l^{2/3}\delta^{4/3}\omega$ in homogeneous turbulence and was verified by our computa-

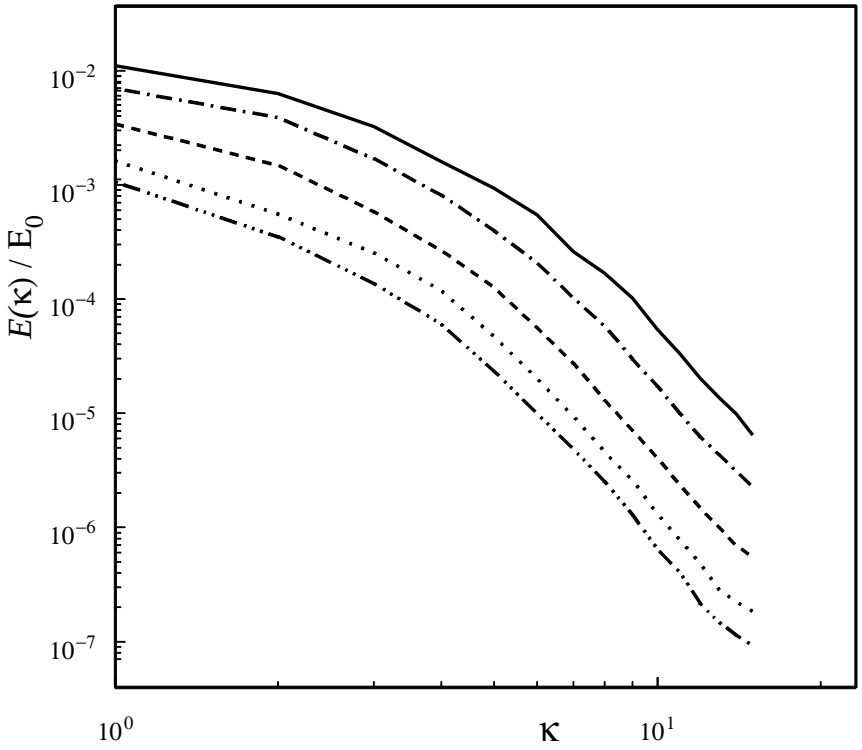

Figure 2.3: One-dimensional energy spectra. Curves at $t/\tau = 2.1$ (——), 4.2 (–·–·–), 10.4 (– – –), 20.8 (· · · · ·), 31.2 (–· · ·–· · ·).

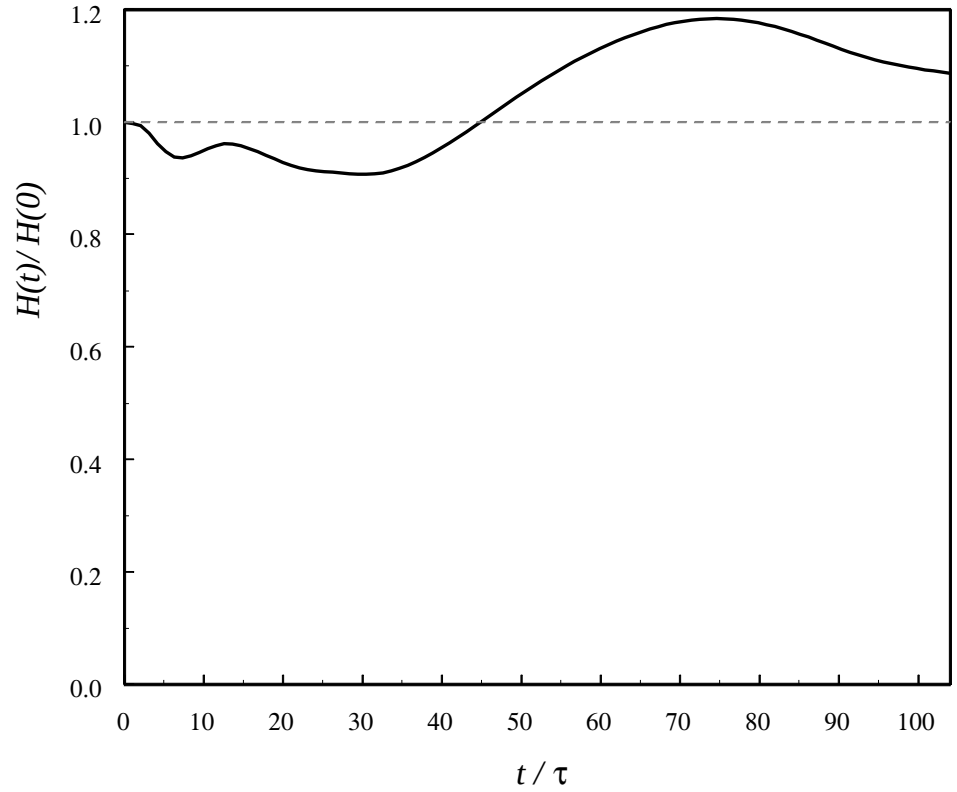

Figure 2.4: Scaling law for angular momentum during the decay, $H(t) = h/(l^{2/3}\delta^{4/3}\omega)$.

tion, confirming the validity of the overall assumptions made in the angular momentum balance equation. Figure 2.4 shows the time evolution of $H(t)/H(0)$, with $H(t) = h/(l^{2/3}\delta^{4/3}\omega)$, where h and ω are computed as the mean modulus of angular momentum and vorticity of the resolved field averaging in the whole domain. Deviations from unity of more than 9% appear only after more than 30 eddy turnover times.

Chapter 3

Shearless turbulence mixings by means of the angular momentum large eddy model

1. Overview

The model introduced in chapter 2 is used to analyze a more complex flow, the mixing of two turbulent fields in the absence of mean shear. It is also a test of the model in a more complex situation. This particular flow configuration allows to enlighten the mechanisms of self-interaction of turbulent flows with different properties without being concealed by other phenomena, in particular by the mean flow shear instabilities. This configuration was first studied by Gilbert (1980), by means of experimental grid turbulence, and later by Veeravalli & Warhaft (1989) again by means of grid turbulence, but with the use of different sets of grids, realizing thus more flow situations, all characterized by a stronger turbulent kinetic energy gradient. The experimental setup consists of a wind tunnel with two grids with the same solidity (to obtain the same mean velocity) but with different size. These two grids with different size produce homogeneous and isotropic flows with different turbulent kinetic energies and different integral scales. A mixing layer then develops between them. In the hypothesis of two homogeneous isotropic turbulent field that are going to mix and high Reynolds numbers, each field is statistically fully defined by two parameters in the Kolmogorov's theory: the turbulent kinetic energy and the integral scale (or the dissipation rate). Thus, two parameters characterize the mixing: the ratio of kinetic energy and the ratio of integral scales.

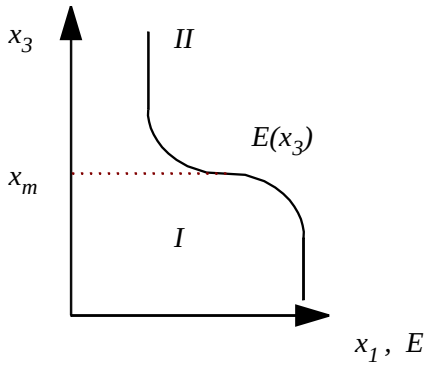

Figure 3.1: Sketch of the mixing configuration.

In experimental investigations these two parameters are not independent, inasmuch as the experimental grid makes that greater scales are always coupled with greater energies. As opposed to them, numerical simulations do not have this limitation, although one has to cope with the problem of generating suitable initial condition.

The only attempt to reproduce these flows, made by Briggs et al. (1996) with a 128^3 direct numerical simulation employing the pseudo-spectral code by Rogallo (Bardina et al. (1983)), was limited by the numerical procedure used to get the initial conditions, which produced flows with the same integral scale. Numerical simulations of this type essentially reproduce a merging of energy and not of integral scales. As a consequence other types of mixings here simulated were envisaged to complete, in this regard, the study of the process of turbulence amalgamation in absence of production.

Three types of mixings of homogeneous and isotropic turbulences in the absence of the production mechanism due to shear are then analyzed. The first realizes an exchange of energy between turbulences with same integral scale, the other two join turbulences with an initial large difference of integral scale either opposite or concurrent to the gradient of turbulent kinetic energy. Unfortunately the literature does not yield results relevant to these last cases, that are entirely new and do not have any comparison.

2. Initial conditions

Numerical simulations of these mixings may be done on a cubic domain with periodic boundary conditions, thus allowing the use of the same code already used for homogeneous turbulence (Briggs et al. (1996)). However, the real

problem to face with is the availability of homogeneous isotropic turbulent flows with the prefixed values of energy and integral scales ratios. The simplest procedure is to start from a realization of a homogeneous turbulent field and then to operate on it to modify its statistical properties. In doing it we take advantage from the availability of the data by Wray (1998) for homogeneous turbulence used for the model validation. This overruns the problems due to the use of random numbers generators to realize turbulent fields. The datasheet by Wray is used as high energy turbulence; in the following, we shall discuss how to obtain the lower energy flow from the higher energy one and how to juxtapose them.

The first case we analyze is the mixing between turbulent flows with the same integral scale. A flow with the different kinetic energy may be simply obtained multiplicating the original one for a constant α:

$$\mathbf{u}^{II}(\mathbf{x}, 0) = \alpha \mathbf{u}^{I}(\mathbf{x}, 0)$$

This modifies energy, which is rescaled by a constant α^2, but does not affect anyway the shape of energy spectra and thus the integral scale ℓ, defined for an homogeneous isotropic flow as

$$\ell(t) = \frac{\int_0^{+\infty} \mathcal{R}_{11}(r, 0, 0, t)\mathrm{d}r}{\mathcal{R}_{11}(0, 0, 0, t)}, \tag{3.1}$$

where $\mathcal{R}_{ij}(\mathbf{r}, t)$ is the velocity fluctuation correlation tensor[1], remains unaltered. This is essentially the way employed by Briggs et al. (1996). Initial conditions of this kind only allow to reproduce a merging of energy but not of integral scales.

To change the integral scale we have to change the shape of energy spectra in the low wavenumbers range, realizing a sort of "filtering" of the velocity field. There are basicly two different ways to change the integral scale in homogeneous isotropic turbulences to be mixed.

The first consists of merging turbulences having decayed over different time intervals. This way has the obvious advantage that the two fields are processed by the equations of motion and then the filtering is a natural one. If the second field is obtained through the decaying of the first one, it will be less energetic and with smaller scales damped out by viscosity. The result is a young, slim and high energy turbulence merged together with an old, low energy and large macroscale turbulence. In such situation one will face a gradient of integral scale always opposite to that of the kinetic energy. This is the second type of mixing we studied.

[1]No primes are used to denote fluctuations because the mean velocity is zero.

The second way of "filtering" consists in directly modifying the spectrum. This is done applying a real filter to the velocity:

$$\hat{\mathbf{u}}^{II}(\mathbf{k},0) = \hat{\mathbf{u}}^{I}(\mathbf{k},0)\hat{g}(\mathbf{k})$$

The initial conditions of the third example of mixing we present belong to this category. In it we subtract energy directly from the smallest wave numbers (the larger scales), with the function $\hat{g}$ chosen as

$$\hat{g}(\mathbf{k}) = \begin{cases} 0 & \text{for} \quad \| \mathbf{k} \| \leq k_1 \\ \dfrac{\| \mathbf{k} \| - k_1}{k_2 - k_1} & \text{for} \quad k_1 \leq \| \mathbf{k} \| \leq k_2 \\ 1 & \text{for} \quad \| \mathbf{k} \| \geq k_2 \end{cases}$$

we obtain a flow with less energy and with a smaller macroscale, thus realizing a mixing with concurrent gradients of both energy and integral scale. Function g as above does not affect the inertial range of turbulence.

These procedures to differentiate energies and integral scales may be combined. For example, a second field with the same energy and different spectrum may be obtained through multiplication by a constant greater than one a decayed turbulence (with a greater scale) or a filtered one (with a smaller scale).

The second step to obtain the initial conditions is to merge these two flows. This is made through a weighting function that artificially creates a smooth transition region between them. Let us call x_3 the non homogeneous direction; the initial velocity field is obtained as

$$\mathbf{u}_*(\mathbf{x},t) = \mathbf{u}^{I}(\mathbf{x},t)p(x_3) + \mathbf{u}^{II}(\mathbf{x},t)(1-p(x_3)) \tag{3.2}$$

where the following function is used

$$p(x_3) = \frac{1}{2}[1 + \tanh(bx_3)\tanh(b(x_3-\pi))\tanh(b(x_3-2\pi))] \tag{3.3}$$

with coefficient $b > 0$. This function may be extended periodically out of $(0, 2\pi)$ as a infinitely smooth function. When applied to the first case, in which the second velocity field is merely a constant multiplying the first one, this procedure is equivalent to multiply $\mathbf{u}^I$ for function $p^*(x_3)$ given by

$$p^*(x_3) = \alpha + \frac{1-\alpha}{2}[1 + \tanh(bx_3))\tanh(b(x_3-\pi))\tanh(b(x_3-2\pi))] \tag{3.4}$$

With regard to the shape function used by Briggs et al. (1996) to modulate the velocity, a Gaussian function extended periodically, our function does

Flow parameters	A	B	C	Veeravalli-Warhaft (3:1 perforated plate)
E_{II}/E_I	0.15	0.017	0.70	0.16
ℓ_{II}/ℓ_I	1	2.7	0.64	
$(\ell_{II}/\ell_I)_k$	0.53	1.9	0.89	0.45
λ_{II}/λ_I	1	8.6	0.77	1.13

High energy region parameters	A,B,C	Veeravalli-Warhaft (3:1 perforated plate)
$E_I\,[\mathrm{m^2 s^{-2}}]$	0.050	0.051
$l_I\,[\mathrm{m}]$	0.048	0.0178
$\lambda_I\,[\mathrm{m}]$	$6.2 \cdot 10^{-3}$	$5.3 \cdot 10^{-3}$
$\tau_I = l/E_I^{\frac{1}{2}}\,[\mathrm{s}]$	0.22	0.078
Re_{ℓ_I}	950	371

Table 3.1: Flow parameters for the four reference mixings; E, ℓ and λ are the turbulent kinetic energy, the integral scale and the Taylor microscale; the subscripts I and II refer to the high and low energy regions, subscript k refers to quantities estimated through the Kolmogorov equilibrium law. The viscosity is $\nu = 1.6 \cdot 10^{-6}\mathrm{m^2 s^{-1}}$. Labels A, B, C refer to mixings without gradient of integral scales, with concorde and opposite gradients of integral scale and energy.

not have only the advantage of preserving the continuity of its derivatives at periodicity boundaries, but it is also able to leave unaltered the two velocity fields outside a thin region of thickness roughly proportional to parameter b, being approximatively constant far from 0, π, 2π.

The resulting velocity given by (3.2) has a non-zero divergence and then must be projected into the space of divergence-free vector functions to enforce continuity. This is made solving a Poisson equation: for Ladyzhenskaya's theorem the space of vector functions may be decomposed as direct sum of the spaces of divergence free and of curl free vector functions,so we can write

$$\mathbf{u}_* = \mathbf{u} + \nabla\phi, \quad \nabla \cdot \mathbf{u} = 0$$

taking the divergence we obtain

$$\nabla^2\phi = \nabla \cdot \mathbf{u}_*$$

Solving this problem we have ϕ and then we are able to know $\mathbf{u} = \mathbf{u}_* - \nabla\phi, \quad \nabla \cdot \mathbf{u} = 0$. This operation leads only to small modifications of the

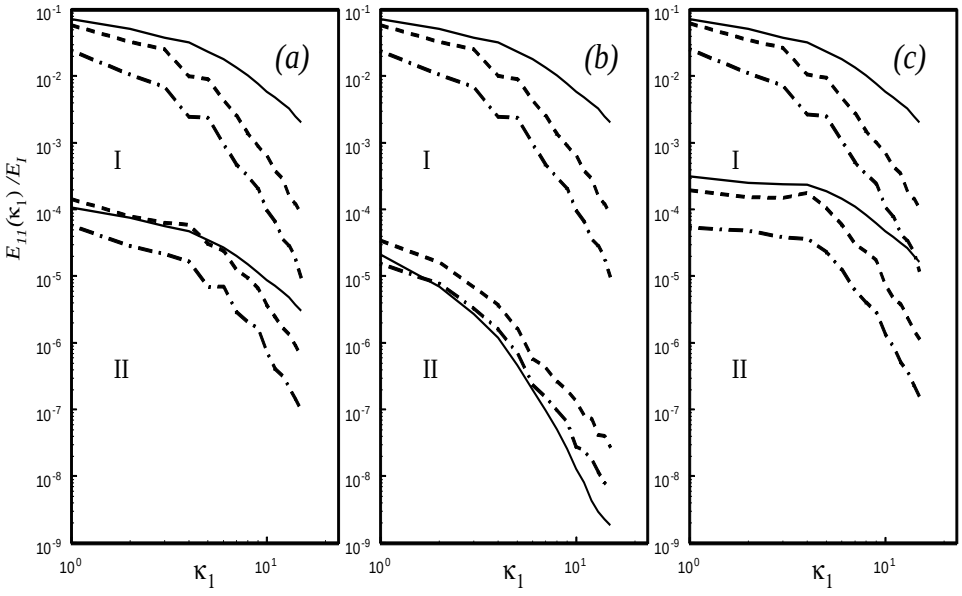

Figure 3.2: Energy spectra for the three reference mixings. Lines are at $t/\tau_I = 0$, 1.1 and 2.2. Low energy region data are offset by 10^{-2}

velocity field in the mixing layer. Then the fields **u** and **h** are computed averaging as stated in section 3.4.

A short remark is needed about the computation of the initial conditions for the angular momentum **h**. In the first and in the last cases we operated directly on the DNS data, so we could calculate it directly from integration, in the same way of previous chapter. In the second case, we were forced to use directly a velocity field obtained as a result of the decay of homogeneous turbulence by means of our large eddy simulation (see previous chapter). We use for **h** the same treatment reserved for **u**. This produces a vector error in the computation of the initial condition for **h** equal to

$$\Delta\mathbf{h} \sim p'(x_3)\delta^2(< u_2^I > - < u_2^{II} >, < u_1^I > - < u_1^{II} >, 0).$$

Flow parameters obtained through these manipulations are summarized in table 4.1 for the three reference situations that will be discussed in the following sections. Energy spectra for the initial stage of evolution are shown in figure 3.2. Additional simulations and further investigations are addressed later.

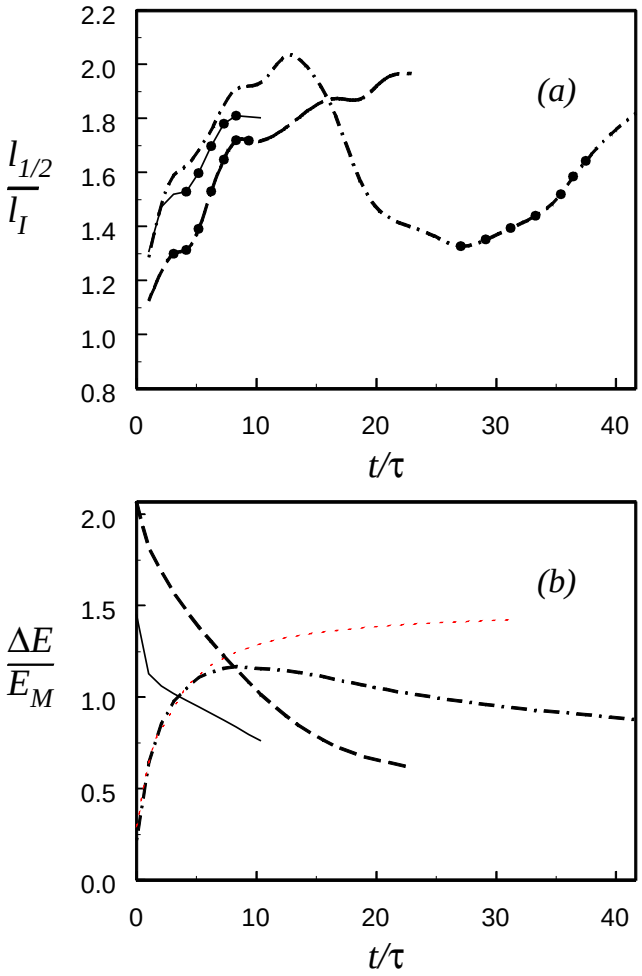

Figure 3.3: Mixing layer thickness (a) and relative dishomogeneity (b) for the first three reference cases A (——), B(– – –), C(– · – · –). Data from indipent evolution of relative energy difference the two fields of case C is also plotted for reference in (b) (· · · · ·). Dots in (a) refer to the self-similarity stage of decay.

3. Mixing without integral scale gradient

The first numerical experiment presents the mixing of turbulences with different turbulent kinetic energies distributed quite similarly over the wave numbers. Field II was obtained from field I after multiplication by a constant, chosen such that the parameters of Veeravalli & Warhaft (1989) (3:1

perforated plate) are reproduced as close as possible. This experiment has already been carried out by Briggs et al. by means of direct numerical simulation and of course in laboratory by means of grids experiments by Veeravalli & Warhaft (1989), in a very detailed and complete manner. As done by Briggs et al. we will use this experiment as the standard comparison reference. Whenever the two mixing field are obtained simply multiplying by a constant an initial velocity field, as done by Briggs et al. (1996) and by us to reproduce their simulation, the numerical experiment is bounded to be an apparent example of mixing of turbulence scales, as we remarked above in our discussion on initial conditions.

Briggs et al. used in their paper approximated values for the integral lengths coming from the hypothesis of statistical equilibrium. However their simulation (cfr. Figure 8, page 225), as well as the experiments of Veeravalli & Warhaft and the present simulation, could not satisfy this hypothesis, since the global Reynolds numbers were too low. The values of Re_ℓ reached were less than 500, that is a typical value today computing machines or laboratory facilities may simulate. With these values relation

$$\ell = \frac{E^{3/2}}{\epsilon}, \tag{3.5}$$

must be replaced by

$$\frac{\ell\epsilon}{E^{3/2}} = f(Re), \tag{3.6}$$

where function f tends toward 1 in the limit for $Re \to \infty$. However, (see Batchelor (1953), page 106) measurements at lower Reynolds numbers with grid turbulence show that f is a roughly decreasing function of Re and its value almost halves when the global Re quadruple from 25 to 107. As a consequence the integral length ratio computed from Kolmogorov may be affected by an error as great as 75 % for a turbulence mixing with a Re ratio near 4. Taking this into account the ratio of integral scales presented by Briggs et al. could change from 1.66 to 0.95 (see there figure 8 and table 1, from which it can be deduced that the ratio between the two Re_ℓ of the turbulences to be mixed is 107/25). For all our simulations, to show the entity of the approximation induced by the adoption of the hypothesis of statistical equilibrium, we have listed in table 1 the ratios of integral scales estimated using both definitions. In the following we always used the values given by the correlation integral.

Note that, even if in principle a laboratory experiment is not affected by this problem because the two merging flows are materially generated by

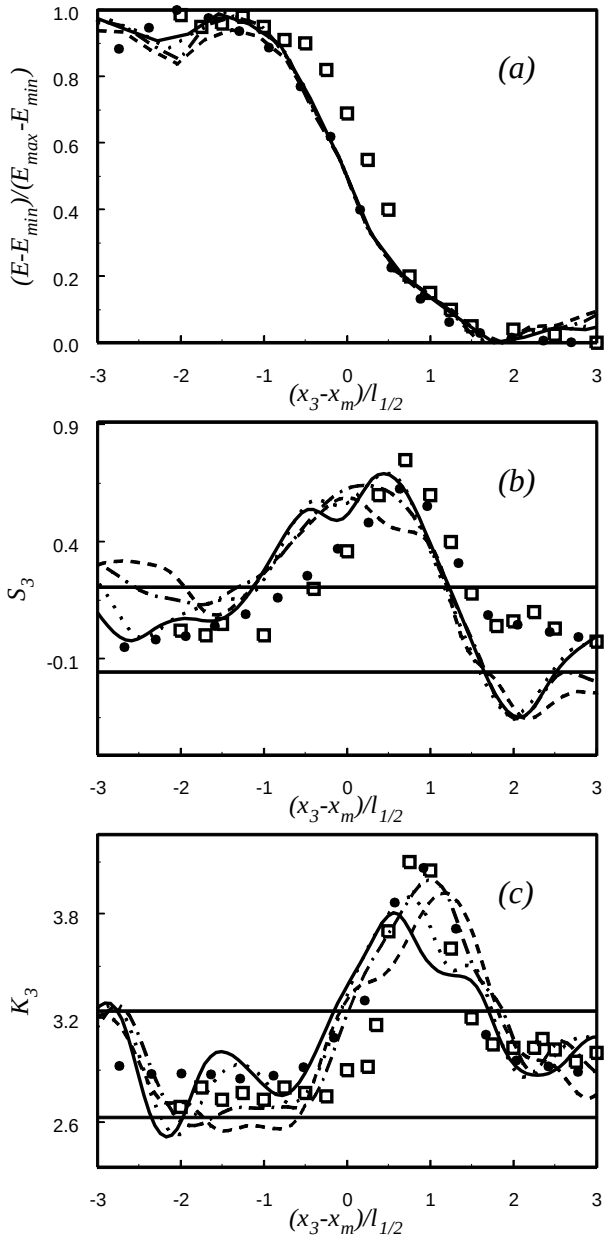

Figure 3.4: Normalized energy, skewness and kurtosis for the mixing without gradient of integral scale (Case A). Curves at $t/\tau_I = 4.2$ (——), 6.3 ($\cdots\cdots$), 8.4 ($-\cdot-\cdot-$), 10.5 ($---$). Dots refer to data by Veeravalli & Warhaft (1989), squares to data by Briggs et al. (1996).

different grids, so that two different integral scales must be present, however the scales estimated through the Kolmogorov law will be in the same way approximated due to the low Re values realized in their facility (cfr. table 1 in Veeravalli & Warhaft) and so the ratio of scales was closer to unity than they extimated. This partially justifies the adoption of their experiments as comparison for the our mixing without gradient of scales.

In treating the results, all statistical averages, denoted in the following with an overbar, are replaced by averages on planes at constant x_3, where coordinate x_3 is along the non-homogeneous direction. The first variable to check in an energy mixing is clearly the kinetic energy, which is used to normalize spatial positions within the mixing layer. A normalized kinetic energy is defined as

$$E^* = \frac{E - E_{min}}{E_{max} - E_{min}}$$

where E_{max} and E_{min} are the maximum and minimum values of the kinetic energy E. As proposed by Veeravalli & Warhaft (1989) and later used by Briggs et al. (1996), we define as centre of the mixing the point x_m where the normalized energy E^* is equal to 1/2, and then a conventional mixing layer thickness $\ell_{1/2}$ as $\ell_{1/2} = \mid x_{0.25} - x_{0.75} \mid$, with $x_{0.25}$ and $x_{0.75}$ the points where E^* is equal to 1/4 and 3/4.

The results we obtained for this mixing case are illustrated in figure 3.3, where the temporal evolution of global quantities as the normalized layer thickness and normalized maximum variation of energy ΔE are plotted, and in figure 3.4, that contains the kinetic energy distributions across the mixing layers at various times of decay together with the distributions of skewness and kurtosis of the transversal fluctuation

$$S_3 = \frac{\overline{u_3^3}}{\overline{u_3^2}^{3/2}}, \quad K_3 = \frac{\overline{u_3^4}}{\overline{u_3^2}^2}.$$

For Gaussian random variables we have $S = 0$ and $K = 3$; even if turbulence is not truly Gaussian Frisch (1995), it does not differ much from these values, that may be kept as reference values. So, the observed deviation may be considered a measure of intermittency.

Our data are in fair agreement with the results both by Veeravalli & Warhaft and by Briggs et al., also plotted for comparison in 3.4. Note that in the paper of the latter, see for example figure 4 there, a systematic energy shift is apparent where the position x_m does not correspond to the definition of mixing centre used also by them. If we perform a shift of their data in order to have $\overline{E} = 1/2$ for $x_3 = x_m$, their statistics collide with ours.

After few eddy turnover times the statistical moments collapse over a typical distribution shape, that remains approximatively unchanged until the mixing process is on. Observing the temporal evolution for many eddy turnover times we reached a state characterized by the flattening of all the distributions. As a consequence a mixing region could no more be recognized. At this point the mixing is under disruption and the entire flow slowly decays towards a new state of uniformity to be asymptotically reached.

The time interval where the mixing shows a near self-similar behaviour lasts in this case about six time units. During it the mixing grows in space while losing energy at a constant rate of 3.3×10^{-2}, see figure 3.3(b). The flow of energy from the high-energy region downward is described by the skewness and kurtosis distributions, see figures 3.4(b), 3.4(c). These are characterized during all the self-similarity interval by values very different from those of the Gaussian equilibrium and present a peak situated in the region of low variance. Anisotropy is thus associated to strong intermittency. As explained in both Veeravalli & Warhaft and Briggs et al., the intermittency is due to energetic eddies penetrating the weak region against the gradient of energy. The normalized position s of this peak is the parameter apt to quantify this penetration distance. In case A its value was 0.7, the transfer of energy having started inside region I at a normalized coordinate $x_3 = -1$ and ended in region II at $x_3 = 1$.

4. Mixing with opposite gradients of integral scale and energy

This second experiment consisted in the mixing of two homogeneous turbulences already decayed over two very different time intervals. The high energy region was Wray's simulation, while the turbulence in the other region was obtained from the data field of region I after a further decay lasting 31 revolving units. So doing we have directly two distinct scales: the old lived turbulence with a large integral scale and low energy, the young turbulence with a small integral scale and a lot more of energy. For the spectra employed to start this mixing case see figure 3.2. The integral scales ratio is $\ell_{II}/\ell_I = 2.7$ (computed according to its definition (3.1)) and the energy ratio $E_{II}/E_I = 1.7 \times 10^{-2}$. Thus the gradient of scales is contrary to that of the kinetic energy. We privileged a high ratio ℓ_{II}/ℓ_I because we wanted to be really sure to mix turbulences with very different integral scale. If we had kept the ratio E_{II}/E_I equals to that of case A we would have got a ratio $\ell_{II}/\ell_I \approx 1.5$. According to the above discussion this value seems too low to enlighten the differences in behaviour obtained through a numerical

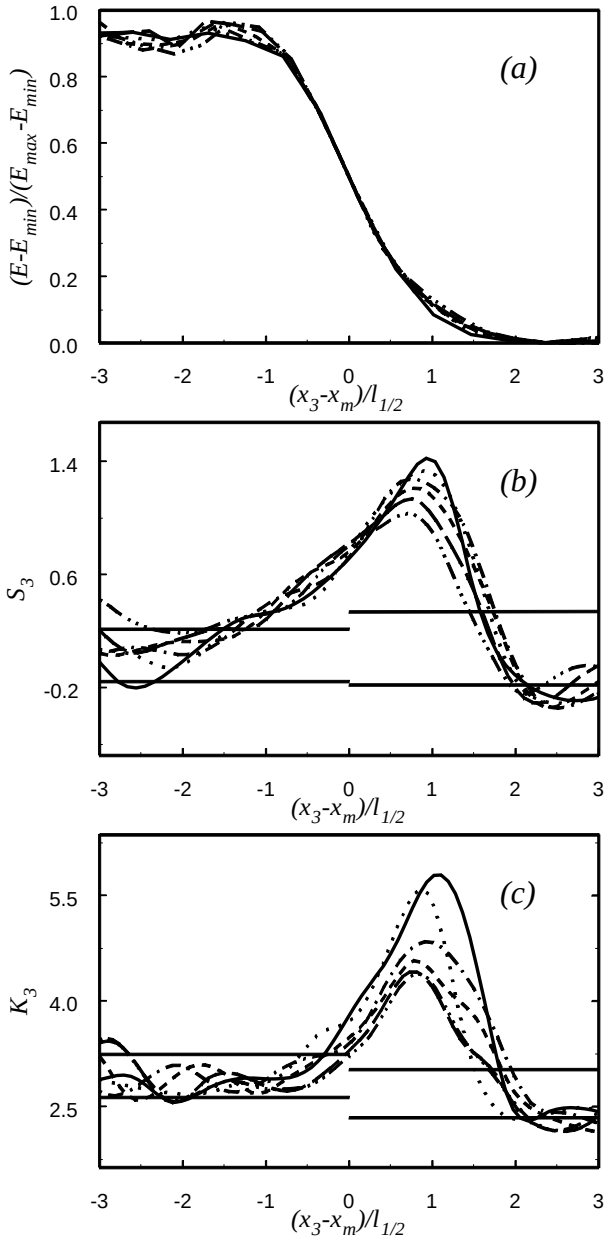

Figure 3.5: Normalized energy (a), skewness (b) and kurtosis (c) for the mixing with gradient of integral scale opposite to that of energy (Case B). Curves at $t/\tau_I = 3.2$ (——), 4.2 ($\cdots\cdots$), 6.3 ($-\cdot-\cdot-$), 9.5 ($---$).

simulation.

This situation of mixing led to a fast and intense flow of energy along the anisotropy direction, since the initial energy difference in the two turbulence undertaking the mixing is very high, see figures 3.3 and 3.5. The normalized decay rate of the mixing, defined as the time derivative of the ratio between energy difference and mean energy of the two flows, is in this case 7.7×10^{-2}, more twice as previous mixing. With regards to case A, the peak value for the skewness distribution doubled, while the kurtosis peak increased of about 50% at the beginning of the decay in the self-similar time interval and then it lowered at a value nearly equal to that of case A. Instead the spatial position of these peaks stayed more or less unchanged with respect to case A, in fact they resulted to be placed at about $0.8 < s < 1$. Thus the penetration of this mixing did not result appreciably higher, notwithstanding an energy ratio higher than the one of the preceding example, where actually the gradient of scales was zero. Schematizing, very fast but small structures are not able to penetrate over long distances whether contrasted by comparatively large, even if very weak, structures. The layer thickness was smaller than in case A, however its temporal growth was similar to that of case A, see figure 3.3(a).

5. Mixing with concurrent gradients of integral scale and energy

This case was the completing numerical experiment of the study about the mixing of turbulences in the lack of the production process of turbulent energy. Here concurrent gradients of energy and scales are considered. Such a situation is obtained merging turbulences that differ in the energy content at the smallest wave numbers, following the procedure described in section 2, with filtering parameters $k_1 = 4$, $k_2 = 6$. Since the two spectra coincide at the high wave numbers, this part of inertial structures is not involved in the energy exchange that will be carried on through the interaction between the largest eddies of regions I and II. In our simulation this process turned out to be very slow and complicate. Looking at figure 3.6(a,b) one sees that the mixing layer grows not self-similarly, up to about 13 eddy turnover times τ_I, beyond which it decreases until $t/\tau_I = 25$, where it restarts the growth showing then self-similarity. Such a behaviour corresponded at first to an oscillating normalized energy flow, after few eddy revolving times this flow became positive and slowly increased until, inside the self-similar interval, it became constant . Thus in the initial transient the two turbulences did not efficiently interact and only entered the phase of constant normalized energy

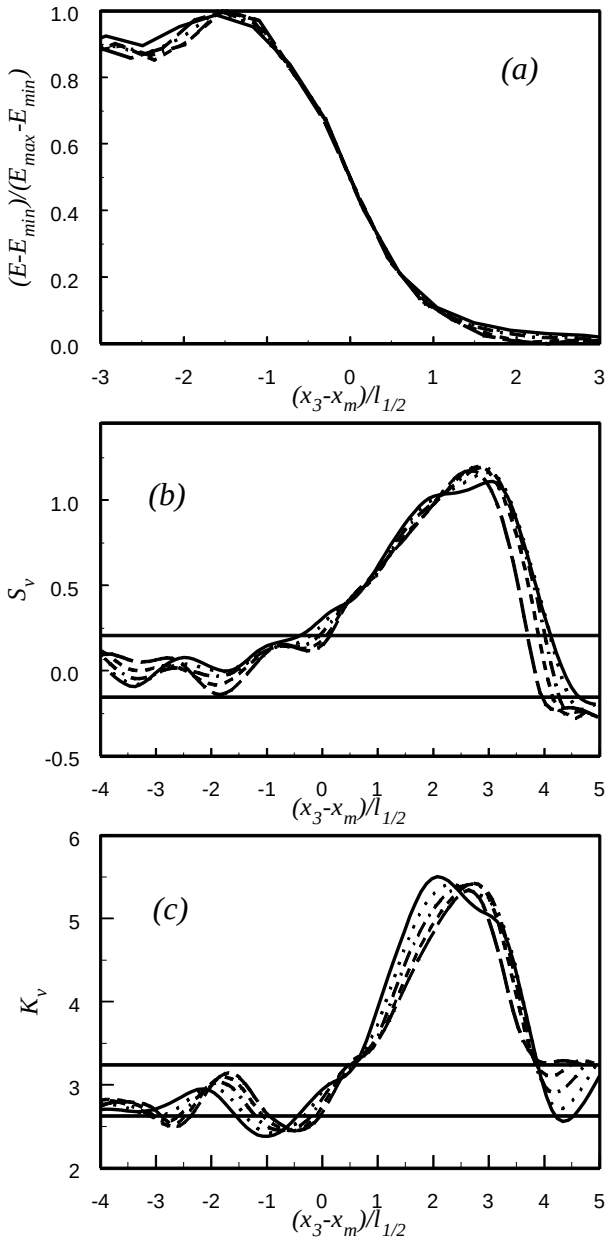

Figure 3.6: Normalized energy (a), skewness (b) and kurtosis (c) for the mixing with gradient of integral scale concurrent to that of energy (Case C). Curves at $t/\tau_I = 26$ (——), 28 (· · · · ·), 30 (–·–·–), 32 (– – –), 34 (—— ——).

transfer at $t/\tau_I = 25$. There the decay rate for $\Delta E/E_M$ was 8.5×10^{-3}, value kept approximatively constant until $t/\tau_I = 38$. The normalized energy difference grew until E_M decreased faster than ΔE ($t/\tau_I \sim 9$), afterwards it decreased because ΔE went down faster than E_M. This should be expected in advance from Kolmogorov's relation between energy, dissipation rate and integral scale. Note that the decay of E_M is not significantly influenced by the process of mixing and that, in the case of independent decay, function $\Delta E/E_M$ is always decreasing, see figure 3.3(b).

This overall conduct recalls some of the lineaments of the instability of a forced Kelvin-Helmoltz laminar layer, see Ho & Huerre (1984), that, contrary to what happens here, is a problem controlled by the instability production mechanism associated to the presence of a mean shear. In particular, the blocked growth of the turbulcence mixing observed in this last mixing reminds of the vortex pairing and the subsequent inhibition of the merging of the paired vortices, phenomenon also leading to the layer growth suppression. After this stage the Kelvin-Helmoltz layer rekeeps the growth. In this case, the interaction is mainly due to the largest eddies and thus the exchanges are markedly slower than previous cases. This is only in part intuitive, because if it is true that the large structures are also the slowest ones, a turbulence amalgamation delay lasting more than 20 revolving times was unexpected. The penetration is very enhanced. Looking figure 3.6 (b,c) one sees that the position s of the peaks of the skewness and kurtosis was now almost triplicated. In this case the more energetic and now larger eddies of region I were displaced for a great distance inside the weak region II. However, it must be remarked that the definition of self-similarity used here is more severe than that of Veeravalli & Warhaft (1989) and Briggs et al. (1996), who considered only self-similarity of energy distributions, while we simultaneously considered a self-similar behaviour of energy, skewness and kurtosis. In fact a self-similar stage of decay is observed for energy long before the self-similarity of skewness and kurtosis and lasts more. For this case of mixing the divergence between angular momentum and vorticity has been checked. In figure 3.7 the path of a particle (part a) crossing the mixing layer is shown, together with the angle between $\mathbf{h}$ and $<\boldsymbol{\omega}>$ and the ratio of their modulus (part b). It is possible to observe as these quantities tend to become very different in presence of strong spatial non homogeneity. Many other particle paths were observed to show a similar behaviour, although they were not enough to a statistically definitive conclusion. Part (a) of this figure contains also a visualization of the slow displacement of the axis of the mixing towards the low energy side of the domain.

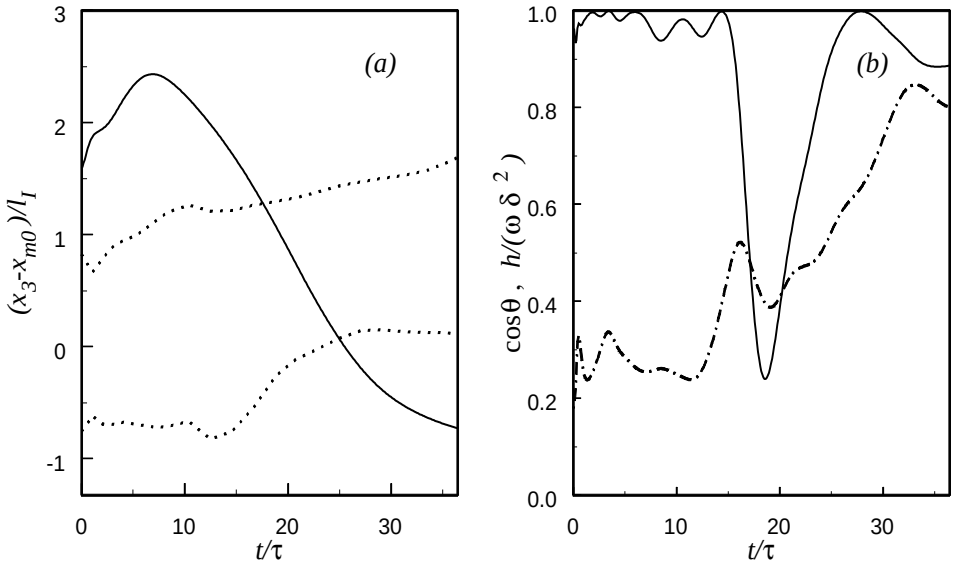

Figure 3.7: (a) path along x_3 of a particle crossing the mixing layer, dotted lines are the positions where the normalized kinetic energy is 0.25 and 0.75 respectively, see §4.3, (b) evolution along the path of the ratio $h/(\delta^2\omega)$ $(-\cdot-\cdot-)$ and of $\cos\theta = (\boldsymbol{\omega}\cdot\mathbf{h})/(\omega h)$ $(——)$.

6. Accuracy estimates

Prior to further discuss our results, a short note on their accuracy is needed. In the numerical procedure that has been used, the periodic boundary conditions create two mixing layers. Due to their growth the two homogeneous regions tend to become even smaller and the extremes of our distributions in figures 3.4, 3.5, 3.6 and 3.8 may be affected by the influence of the second mixing layer and must not be relied upon. This effect is not significant with the exception of case C of previous section, in which the simulation was carried out for much longer times and we observed greater mixing thickness.

Accuracy estimates for our simulation are deduced *a posteriori* for this set of numerical simulations. The source of all the turbulence fields that were used was the direct numerical simulation of homogeneous and isotropic turbulence by Wray (1998) (see section 2). The raw data by Wray, after the preliminar filtering and before computing the mixing by LES method, presented a dishomogenity level of about $\pm 8\%$ (maximum variation of kinetic energy with respect to the average kinetic energy) and skewness and kurtosis values slightly different from that of the statistical equilibrium (respectively 0.02 ± 0.2 instead of 0 and 2.9 ± 0.3 instead of 3) when averages are taken on planes at constant x_3. Our simulations kept these characteristics. Checking the temporal evolution of the statistical properties of the parts of the field placed outside the mixing and, so by hypothesis still in equilibrium, we found for the kinetic energy distribution a dishomogeneity of about $\pm 5\%$ at $t/\tau_I = 10$ and of $\pm 7\%$ at $t/\tau_I \approx 30$. For the skewness and kurtosis the largest displacement with respect to the equilibrium canonical values was observed in case of the mixing with integral scale gradient opposite to that of energy, where the old lived turbulence ($t/\tau_I = 31$) was one of the mixing turbulences. Here in region II, outside the mixing, we found $S_3 = 0.07 \pm 0.27$ and $K_3 = 2.7 \pm 0.35$. Horizontal lines in figure 3.4, 3.5, 3.6 and 3.8 refer to this ranges of values. Tests with an enhanced spatial resolution (48^3 and 64^3 points), but with the same filter width, confirmed the values reported above about homogeneity and only minor changes about characterizing quantities, showing that the numerical resolution was sufficient to comply with the filtering length. In case A, for example, the difference in the peaks of skewness and kurtosis resulted less than 4%.

These considerations should be kept in mind when analyzing these results.

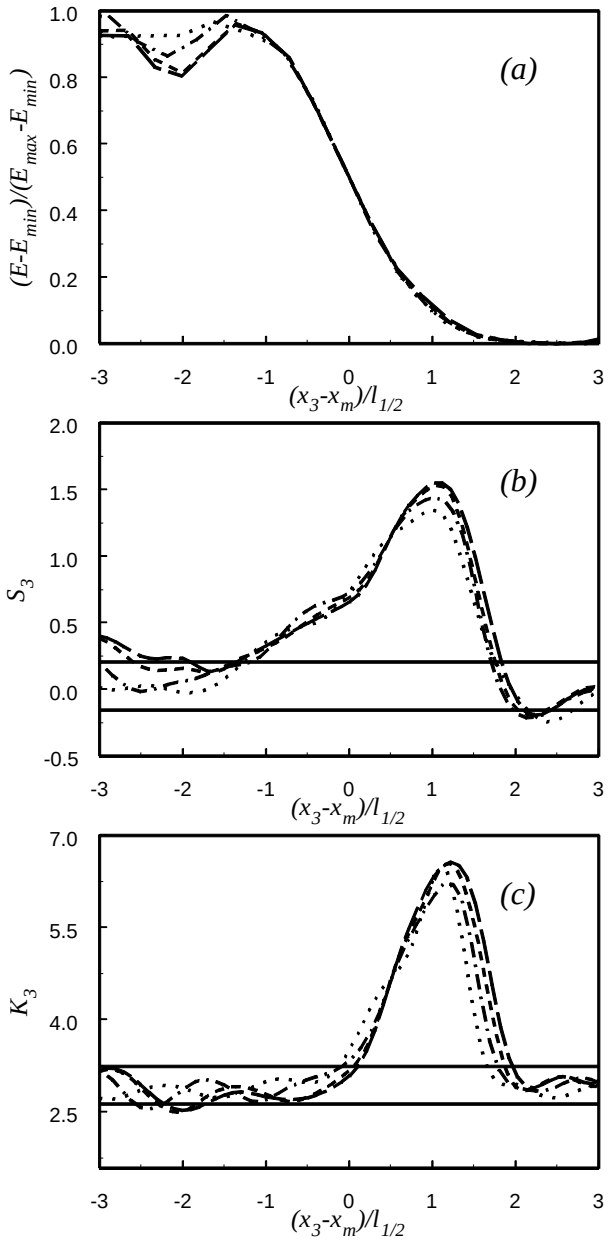

Figure 3.8: Normalized energy, skewness and kurtosis for the mixing without gradient of integral scale and $E_I/E_{II} = 58$. Curves at $t/\tau_I = 4.2$ (——), 6.3 ($\cdots\cdots$), 8.4 ($-\cdot-\cdot-$), 9.5 ($---$).

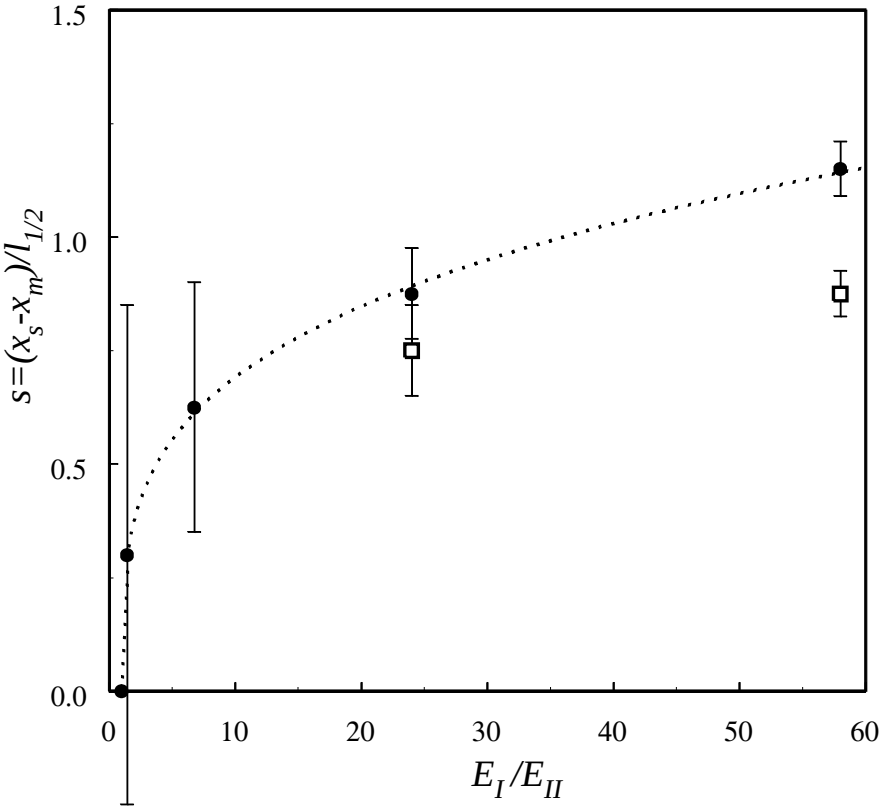

Figure 3.9: Intermittent penetration for different initial parameters. Dots refers to mixings without gradient of integral scales, squares to mixings with an adverse gradient of integral scales; $\ell_{II}/\ell_I = 1.9$ (left) and 2.7 (right) respectively. Estimated errors are also reported.

7. Discussion

To complete the characterization of shearless mixings other simulations were carried out to have a more quantitative evaluation of the dependence of the global features of these mixings on the two parameters involved: the initial ratio of energies and the initial ratio of integral scales. Quantities investigated and compared were skewness' peak positions, energy difference decay and spectra.

The first feature we investigated was the dependence of the penetration on the ratio of kinetic energy. As discussed above, the position of the peaks of skewness and kurtosis is a variable apt to quantify it. In this end we

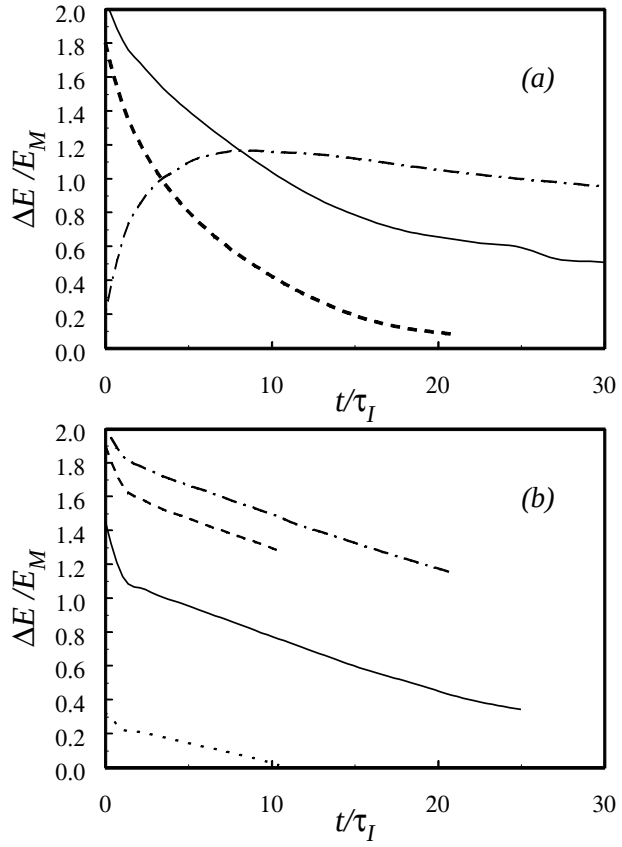

Figure 3.10: Decay of energy difference. (a) Mixings with gradient of integral scale: (—) $E_I/E_{II} = 58$, $\ell_{II}/\ell_I = 2.7$, (– – –) $E_I/E_{II} = 24$, $\ell_{II}/\ell_I = 1.9$, (– · – · –) $E_I/E_{II} = 1.43$, $\ell_{II}/\ell_I = 0.64$. (b) Mixings without gradient of integral scale: (· · · · ·) $E_I/E_{II} = 1.43$, (——) $E_I/E_{II} = 6.7$, (– – –) $E_I/E_{II} = 24$, (– · – · –) $E_I/E_{II} = 58$.

started from the mixing between turbulences with the same integral scale, and repeated the simulation for the additional values $E_I/E_{II} = 1.4$, 24, 58. The last one has the same energy ratio of the mixing with an older turbulence (see section 4.4) and its statistics are reported in figure 3.8, to be compared with figures 3.4 and 3.5, while the first one reproduces early experiments by Gilbert (1980). He could not see any significant variation, attributable to the mixing process, of skewness and kurtosis with respect to values outside the mixing layer due to the small difference of energy characterizing his experiment.

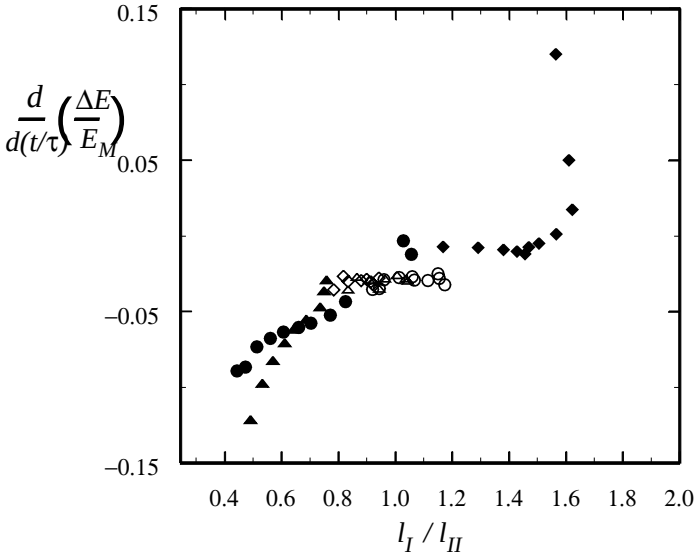

Figure 3.11: Normalized energy difference decay rate versus instantaneous integral scale ratio different mixing configurations. Mixings without gradient of scales: $E_I/E_{II} = 6.7$ ($\circ$), $E_I/E_{II} = 24$ ($\triangle$), $E_I/E_{II} = 58$ ($\diamond$). Mixings with gradient of scales: $E_I/E_{II} = 1.43$ and $\ell_{II}/\ell_I = 0.64$ ($\diamond$), $E_I/E_{II} = 24$ and $\ell_{II}/\ell_I = 1.9$ ($\triangle$), $E_I/E_{II} = 58$ and $\ell_{II}/\ell_I = 2.7$ ($\bullet$).

In effect our simulation meets the same difficulty in identifying both the mixing centre and the position of the peaks. This explains the great error bar in the corresponding point in figure 3.9. This figure shows the position of these peaks in these simulations. Results about these mixings between turbulences with the same spectral characteristics fit in with a power law

$$s = a\left(\frac{E_I}{E_{II}}\right)^b$$

with $a = 0.40$, $b = 0.27$. In this figure we report also results from the two mixings with opposite gradients of energy and integral scale (that of section 4.4 (case B), with $\ell_{II}/\ell_I = 2.7$, $E_I/E_{II} = 58$ and an additional case with $\ell_{II}/\ell_I = 2.0$, $E_I/E_{II} = 24$). Points referring to them are both below the curve, showing the effect of an adverse gradient of scale in reducing penetration. Instead, the only simulation we performed with parallel gradients of energy and scales, with $s \approx 2.6$ would lie far above the curve.

Figure 3.10 shows the time evolution of the relative dishomogeneity $\Delta E/E_M$ between the two turbulent fields that are mixing. We note that

all mixing without initial gradient of integral scale show a linear decrement, at least in the region of self-similarity, with almost the same decay rate. Instead, all the other cases show different decay rates, that appear to be smaller if $\ell_I/\ell_{II} < 1$, greater in the opposite situation.

This suggests a relation between the rate of decay of the normalized energy difference and the ratio of integral scales. So, the relative variations of istantaneous integral scales were investigated. It must be remarked at first that they are not easy to compute, due to limitations in the spatial domain on which averages are computed. This is not due to low numerical resolution of the simulations, but only to the choice to average on planes at constant x_3. In fact, the same problem was faced by Briggs et al. (1996) with their 128^3-DNS, and they were not able, by their explicit admission, to compute one-dymensional spectra smooth enough to obtain reliable integral scales. They finally reverted to an approximate deduction from Kolmogorov. We overcame the problem simply averaging on a greater domain, that is, on the whole high- and low-energy regions outside the mixing layers. In this way the possibility of investigating the variations of ℓ in the mixing layer was lost, but we were able to have reliable estimates of ℓ in the two regions.

In figure 3.11 the decay rate of relative energy difference versus the instantaneous ratio of integral scales is plotted. As the mixing goes on, the ratio ℓ_I/ℓ_{II} tends towards unity, but it still remains significantly different from one in the self-similarity time interval. In the same time the decay rate approaches the values for the mixing without gradient of integral scale. Values for the case with initial ratio ℓ_I/ℓ_{II} equal to one are plotted as reference. We note that, notwithstanding our procedure to compute integral scales, a not negligible dispersion in the data is still present.

Finally, the anisotropy in the mixing layer was investigated. We observed that anisotropy is relevant only to energy flow contributions, because the three components of velocity are all equally significant in the whole flow, with differences limited to less than 10%. This confirms the result shown by the simulation by Briggs, Ferziger et al. (1996). Instead, we found that the energy flow has a very different behaviour, that is a general feature present in every kind of mixing. In the self-similar interval and also outside it, about half the energy flow per unit surface along the non-homogeneous direction $\overline{u_1^2 u_3 + u_2^2 u_3 + u_3^3}$ was contributed by the velocity fluctuations in the x_3 direction (that is, from $\overline{u_3^3}$), while the other two directions roughly equally contributed to the remaining half, as it must be because they are equivalent. Figure 3.12 shows the different contributions to energy flow in different points at different istants for a single case, while figure 3.13 shows the time evolution of relative contributions of the u_3 to the total energy flow

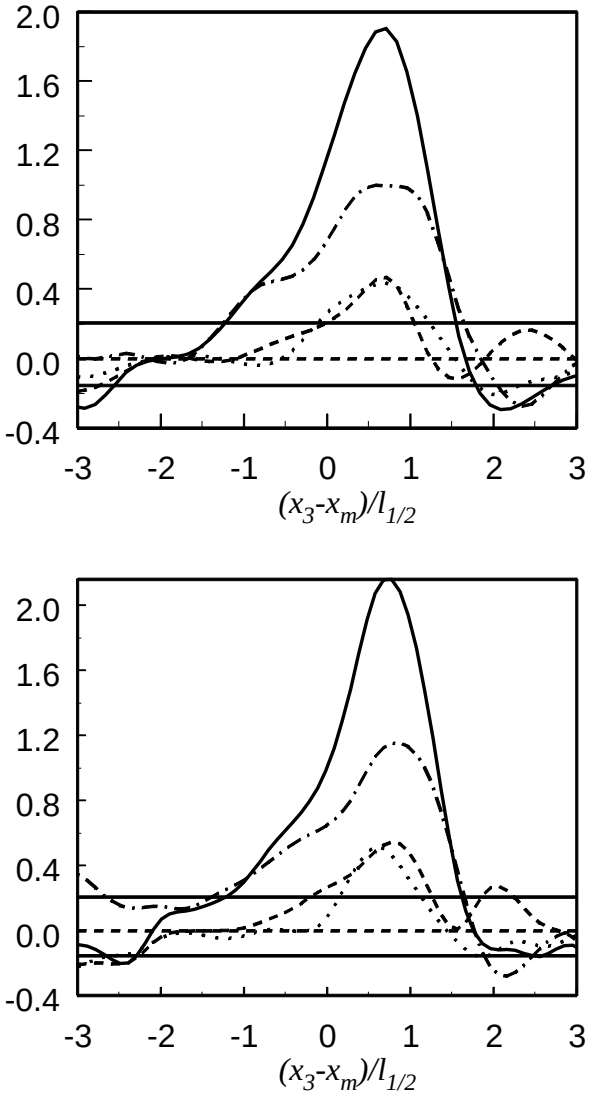

Figure 3.12: Energy flow anisotropy: normalized energy flow contribution at $t/\tau_I = 4.2$ (above) and $t/\tau_I = 8.4$ (below) for the mixing without gradient of integral scales and $E_I/E_{II} = 24$. Curves are for $\overline{u_1^2 u_3}/\overline{u_3^2}^{\frac{3}{2}}$ ($---$), $\overline{u_2^2 u_3}/\overline{u_3^2}^{\frac{3}{2}}$ ($\cdots\cdots$), $\overline{u_3^3}/\overline{u_3^2}^{\frac{3}{2}}$ ($-\cdot-\cdot-$) and their sum (——).

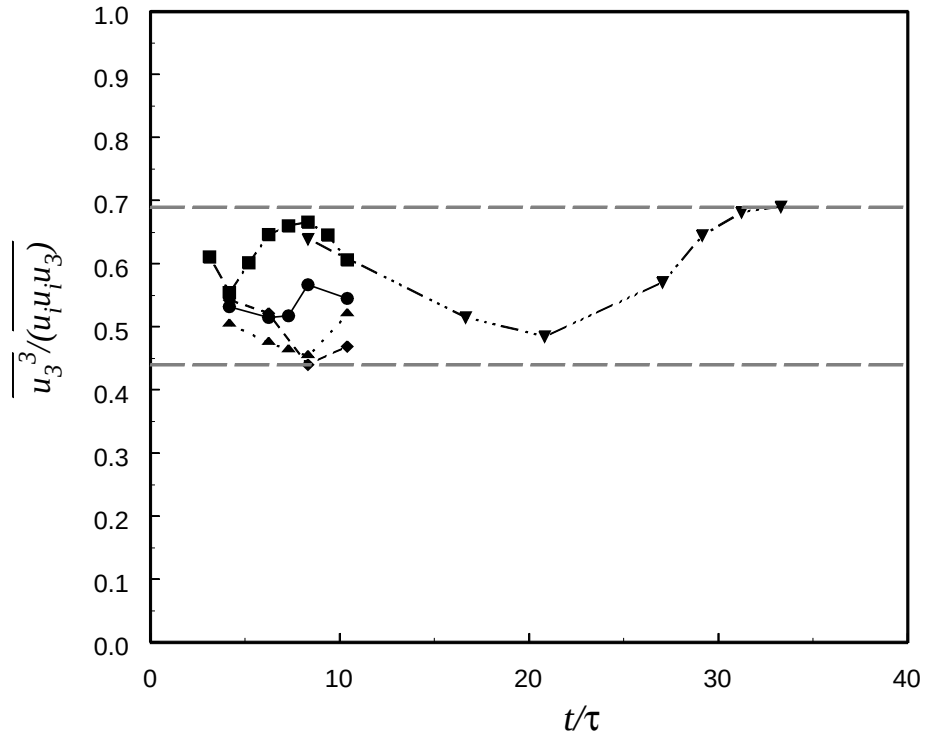

Figure 3.13: Energy flow anisotropy: contribution of the velocity component along the non homogeneous direction to the total energy flow. Curves for mixings without gradient of scales and $E_I/E_{II} = 6.7$ ($-\cdot-\cdot-$), $E_I/E_{II} = 24$ (——), $E_I/E_{II} = 58$ ($\cdots\cdots$) and with gradient of scales, $E_I/E_{II} = 58$, $\ell_{II}/\ell_I = 2.7$ ($---$) and $E_I/E_{II} = 1.43$, $\ell_{II}/\ell_I = 0.64$ ($-\cdots-\cdots$) are reported. Except for the latter case, points are all in the self-similar stage of decay.

for different mixings. They are evaluated in correspondence with the peak of skewness and kurtosis, in corrispondence of the maximum dishomogeneity. In cases A and B such a redistribution - at the initial instant of merging all the components of the velocity fluctuation clearly must equally contribute - was reached in only two eddy turnover times.

Conclusions

The role of angular momentum and the symmetry of flow tensors in fluid dynamics is discussed. It is remarked that the flow symmetry property may be broken only by the simultaneous presence of various causes: presence of the fluid of extended particles owing inertia with external couples acting selectively only on them; rough collision interaction in case of flow of grains (with finite dimension), non local and non central interaction at the subcontinuum level. In such situations the momentum and moment of momentum balances are physically coupled through the antisymmetric part of the stress tensor. Special continuum theories, like the micropolar fluids, were developed to represent this situations and were also used for turbulent flows. It was shown that, inasmuch as any spatial filtering is not able to introduce asymmetries in homogeneous flows, even in turbulent motion, the application of model suited to structured flow field directly to turbulent motions of a homogenous fluid is not justified.

A novel representation of the angular momentum balance in terms of an infinite sequence of independent differential equations operating on the momentum has been determined. These equations may be viewed as higher order vorticity balances. They could be useful to describe the evolutions of the correlation variable coming from the filtering of the equations for the turbulent motion.

Based on the assumption of a turbulence transport coefficient proportional to the intrinsic angular momentum, a large eddy scale turbulent model, which would have possible extensions to flows containing a dispersion of generally shaped particles, provided with inertia or submitted to external couples is proposed. When applied to incompressible flows, this model shows anyway a proper scaling with both the integral and filtering lengths, eventually leading to the independence of the subgrid coefficient from the filtering length. This property may turn out of some convenience for numerical simulation of non structured flows. The model validation is extensive and comprehends a priori test and the simulation of homogeneous isotropic

decaying turbulence.

This new model was applied to shearless turbulence mixings. Simulations of mixings between fields with the same integral scale are in fair agreement with previous results. Also different qualitative configurations not present in the literature were analyzed and the differences of the characteristics of these mixings once the spectral properties of the two merging fields are differentiated changing the integral scale were showed. Two limiting situations are then possible: - mixing between a young energetic (smaller scale) turbulence and an old slow (larger scale) turbulence, in which case the energy flow is inevitably opposite to the gradient of integral scale, - mixing between fields filtered one from the other by reducing the energy associated to the smallest wave numbers, in which case the energy flow is concurrent to the gradient of integral scale. In the first the self-similarity was quickly reached, the exchange of energy was very fast and intense, but the lateral intermittent penetration into the low energy side of the mixing was on the average not much changed with respect to the case where the mixing process involved only the energy and not the integral scale. In the second case a slow evolution was taking place where the layer thickness grew, then diminished and then again started to grow, in the end assuming a self-similar behaviour. The penetration resulted enhanced a lot: the high energy structures were also the largest ones and the position of the maximum of intermittency and normalized energy exchange was displaced three times more.

Bibliography

Almog Y., Brenner H. 1999 Ensemble-average versus suspension scale Cauchy continuum mechanical definition of stress in polarized suspensions: Global homogeneization of a dilute suspension of dipolar spherical particles. *Physics of Fluids*, **11**, 268–273.

Araki S., Tremaine S. 1986 The Dynamics of dense particle disks. *Icarus*, **65**, 83–109.

Bardina J., Ferziger J. H., Reynolds. W. C. 1983 Improved turbulence models based on large eddy simulation of homogeneous, incompressible, turbulent flows. *Report Tf-19*, Stanford University.

Batchelor G. K. 1967 *An introduction to Fluid Mechanics.* Cambridge University Press.

Batchelor G. K. 1953 *The Theory of Homogeneous Turbulence.* Cambridge University Press.

Batchelor G. K. 1970 The stress system in a suspension of free-force particles. *J.Fluid Mech.*, **44**, 545–592.

Brenner H. 1970 Rheology of two-phase systems. *Ann.Rev.Fluid Mech.*, **2**, 137–176.

Briggs D. A., Ferziger J. H., Koseff J. R., Monismith S. G. 1996 Entrainment in a shear-free turbulent mixing layer. *J. Fluid Mech.* **310**, 215–241.

Brigham E. O. 1974 *The fast Fourier transform*. Prentice-Hall, Englewood Cliffs.

Canuto C., Hussaini. M. Y., Quarteroni. A., Zang. T. A. 1988 *Spectral methods in fluid dynamics.* Springer Verlag, Berlin.

Cercignani C., Lampis M. 1988 Kinetic theory of a dense gas. *J.Stat.Phys.*, **53**, 655–672.

Chatwin P. C. 1973 The Vorticity equation as an angular momentum equation. *Proc. Camb. Phil. Soc.* **74**, 365–367.

Clark R. A., Ferziger J. H., Reynolds W. C. 1979 Evaluation of subgrid-scale models using an accurately simulated turbulent flow *J. Fluid Mech.* **91**, 1–16.

Comte-Bellot G., Corrsin. S. 1971 Simple eulerian time correlation of full and narrow-band velocity signals in grid-generated isotropic turbulence. *J.Fluid Mech.* **48**, 273–337.

CONDIFF D. W., DAHLER J. S. 1964 Fluid mechanical aspects of antisymmetric stress. *Phys.Fluids*, **7**, 842.

DAHLER J. S., SCRIVEN L. E. 1963 Theory of structured continua: general consideration of angular momentum and polarization. *Proc. Roy. Soc.*, **A275**, 504–527.

ERINGEN A. C. 1964 Simple microfluids. *Int.J.Eng.Sci.*, **1**, 205–233.

ERINGEN A. C. 1966 Micropolar Fluids. *J.Math.Mech.*, **16**, 1–16.

ERINGEN A. C. 1972 Micromorphic description of turbulent channel flow. *J.Math.Anal. Appl.*, **39**, 253–266.

ERINGEN A. C. 1992 Balance laws for micromorphic media revisited. *Int.J.eng.Sci.*, **30**, 527.

FERRARI C. 1972 Sulle equazioni differenziali di flussi turbolenti. Ist.Naz.Alta Mat., *Symposia Mathematica*, **IX**.

FERZIGER J. H. 1977 Large eddy simulation of turbulent flows. *AIAA Journal* **15**, n.9.

FERZIGER J. H. 1985 Large eddy simulation: its role in turbulence research. In *Theoretical approches to turbulence* ed. A. Hussaini, pp.51–83, Springer Verlag, Berlin.

FRISCH U. 1995 *Turbulence*, Cambridge University Press.

FREZZOTTI A. 1998 Applications of Enskog theory to the study of granular fluids. *21th International Symposium on Rarefied Gas Dynamics*, Marseille.

GERMANO M. 1991 A rate equation for eddy viscosity *Nota scientifica e tecnica N^o 142.*, Politecnico di Torino.

GERMANO M. 1992 Turbulence, the filtering approach. *J. Fluid Mech.* **236**, 325–336.

GILBERT B. 1980 Diffusion mixing in grid turbulence without mean shear *J. Fluid Mech.* **100**, 396–398.

GHOSAL S., MOIN P. 1995 The basic equations for large eddy simulation of turbulent flows in complex geometries. *J.Comp.Phys.* **118**, 24–37.

GOLDSHTEIN, A., SHAPIRO M. 1995 Mechanics of collisional motion of granular materials. *J.Fluid Mech.*, 282, 75–114.

GURTIN M. 1981 *An introduction to continuum mechanics*, Academic Press.

HO C. M., HUERRE P. 1984 Perturbed free shear layers *Ann. Rev. Fluid Mech* **16**, 365–424.

IOVIENO M., TORDELLA D. 1999 Shearless turbulence mixings by means of the angular momentum large eddy model, *American Physical Society - 52th DFD Annual Meeting.*

IOVIENO M., TORDELLA D. 2001 Sviluppo di un codice spettrale per le equazioni di Navier-Stokes incompressibili, *Nota Scientifica e Tecnica DIASP N^o 186*.

JAMESON A., SCHMIDT H., TURKEL E. 1981 Numerical solutions of the Euler equations by finite volume methods using Runge-Kutta stepping schemes. *AIAA Paper* N. 81-1259.

LANDAU L. D., LIFSHITZ E. M. 1983 *Fluid Mechanics.* Pergamon, Oxford.

Laufer J. 1951 Investigation of turbulent flow in two-dimensional channel. *NASA TR-1053*.

Leslie D. C., Quarini G.L. 1979 The application of turbulence theory to the formulation of subgrid modelling procedures. *J. Fluid Mech.*, **91**, 65–91.

Leonard A. 1974 On the energy cascade in large eddy simulation of turbulent flows. *Adv. in Geophys.* **A18**, 237–248.

Lesieur M., Métais O. 1996 New Trends in large eddy simulations of turbulence. *Ann. Rev. Fluid Mech.* **28**, 45–83.

Łukaszewicz, G. 1999 *Micropolar Fluids*. Birkhäuser, Basel.

McMillan O. J., Ferziger J.H. 1979 Direct testing of subgrid-scale models. *AIAA Journal*, **17**, 1340-1346.

Mason P. J. 1992 Large eddy simulation: a critical review of the technique. *Q.J.R.Meteorol.Soc.* **120**, 1–26.

Mattioli G. D. 1933 Sur la thèorie de la turbulence dans les canaux. *C.Rendus Acac.Sci.*, **196**, 1282.

Mattioli, G. D. 1937 *Teoria dinamica dei regimi fluidi turbolenti*. Cedam, Padova, 1937.

Maxwell G. B. 1857 On the stability of the motion of Saturn's rings. *Proc.Roy.Soc.Edinburgh*, **IV**, 290–374.

Moin P., Kim J. 1982 Numerical investigation of turbulent channel flow. *J.Fluid Mech.* **118**, 341–377.

Nee V. W., Kovasznay L. S. G. 1969 Simple phenomenological theory of Turbulent Shear Flows. *The Physics of Fluids* **12**, n.3, 473–484.

Nigmatulin R. N., Nikolaevsky V. N.. 1970 Diffusion of vorticity and the balance of momentum of momentum in dynamics of nonpolar fluids. *Appl.Math.Mech.*, **34**, 318–323.

Nikolaevsky, V. N. 1970 Asymmetric mechanics of turbulent flows. *Appl.Math.Mech.*, **34**, 514–525.

Nikolaevsky V. N. 1973 Asymmetric mechanics of turbulent flows: energy and entropy. *Appl.Math.Mech.*, **37**, 94–105.

Peyret R. 1999 Introduction to high-order approximation methods for computational fluid dynamics. *Prèpublication n^o 543*, Universite de Nice-Sophia Antipolis .

Piomelli U., Ferziger J. & Moin P. 1989 New approximate boundary conditions for large eddy simulations of wall-bounded flows. *The Physics of Fluids A* **1**, n.6, 1061–1068.

Rajagopalan S., Antonia R.A. 1979 Some properties of the large structure in a fully developed duct flow. *Physics of Fluids* **22**, n.4, 614–622.

Rudin W. 1974 *Analisi reale e complessa*. Bollati-Boringhieri, Torino.

Salo, H. 1995 Simulations of dense planetary rings. *Icarus*, **117**, 187–312.

Schumann U. 1975 Subgrid scale model for finite difference simulations of turbulent flows in plane channels and anuli. *J.Comput.Phys.*, **18**, 376–404.

SMAGORINSKY J. 1963 General circulation experiments with the primitive equations. *Monthly Weather Review* **91**, 99–164.

SPEZIALE C.G. 1991 Analytical methods for the development of Reynolds-Stress closures in turbulence. *Ann. Rev. Fluid Mech.* **23**, 107–157.

SPEZIALE C.G. 1992 The energy decay in self-preserving isotropic turbulence revisited. *J. Fluid Mech.* **241**, 645–667.

TENNEKES H. LUMLEY J. L. 1972 *A first course in turbulence.* MIT Press, Cambridge.

TÖZEREN, A. AND R. SKALAK. 1977 Micropolar fluids as models for suspensions of rigid spheres. *Int.J.Eng.Sci.*, **15**, 511–524.

TRITTON D. J. 1987 *Physical fluid dynamics*, Pergamon Press, Oxford.

UNGARISCH M. 1999 *Hydrodynamics of suspensions*, Springer, Berlin.

VAN DRIEST E. R. 1956 On turbulent flow near a wall. *J. Aero. Sci.* **23**, 1007–1011.

VEERAVALLI S., WARHAFT Z. 1989 The shearless turbulence mixing layer. *J. Fluid Mech.* **207**, 191–229.

WISDOM J., TREMAINE S. 1988 Local simulations of planetary rings. *The Astronomical Journal*, **95**, 925–940.

WRAY A.A. 1998 Decaying Isotropic Turbulence. In *AGARD-AR-345 A Selection of Test Cases for the Validation of Large-Eddy Simulations of Turbulent Flows* **207**, Data Sheets for Homogeneous Flows, HOM02, 63–64.

YAGLOM A. S., MONIN A. M. 1975 *Statistical fluid mechanics*, vol.2. MIT Press, Cambridge.

YOSHIZAWA A. 1982 A statistically derived subgrid model for the large eddy simulation of turbulence, *Phys. Fluids*, **25**, 1532–1538.